

Bayesian Quantile Regression with Subset Selection: A Decision Analysis Perspective

Joseph Feldman

Department of Statistical Science, Duke University

and

Daniel R. Kowal

Department of Statistics and Data Science, Cornell University

Department of Statistics, Rice University

Abstract

Quantile regression is a powerful tool for inferring how covariates affect specific percentiles of the response distribution. Existing methods either estimate conditional quantiles separately for each quantile of interest or estimate the entire conditional distribution using semi- or non-parametric models. The former often produce inadequate models for real data and do not share information across quantiles, while the latter are characterized by complex and constrained models that can be difficult to interpret and computationally inefficient. Neither approach is well-suited for quantile-specific subset selection. Instead, we pose the fundamental problems of linear quantile estimation, uncertainty quantification, and subset selection from a Bayesian decision analysis perspective. For any Bayesian regression model—including, but not limited to existing Bayesian quantile regression models—we derive optimal point estimates, interpretable uncertainty quantification, and scalable subset selection techniques for all model-based conditional quantiles. Our approach introduces a quantile-focused squared error loss that enables efficient, closed-form computing and maintains a close relationship with Wasserstein-based density estimation. In an extensive simulation study, our methods demonstrate substantial gains in quantile estimation accuracy, inference, and variable selection over frequentist and Bayesian competitors. We use these tools to identify and quantify the heterogeneous impacts of multiple social stressors and environmental exposures on educational outcomes across the full spectrum of low-, medium-, and high-achieving students in North Carolina.

Variable selection, interpretable machine learning, Bayesian inference, robust regression

1 Introduction

Quantile regression estimates the functional relationship between covariates and specific percentiles of a response variable. In linear quantile regression, the τ th conditional quantile for a random variable Y is modeled as a function of p -dimensional predictors \mathbf{x} via

$$Q_\tau\{Y \mid \mathbf{x}, \boldsymbol{\beta}(\tau)\} = \mathbf{x}^\top \boldsymbol{\beta}(\tau) \quad (1)$$

(a nonlinear version is in Section 2.4). Estimated across τ , the coefficients $\boldsymbol{\beta}(\tau)$ summarize how the covariates affect not only the location, but also the shape of the response distribution $Y \mid \mathbf{x}$. The unique insight from linear quantile regression comes from identifying predictors with *heterogeneous* effects $\beta_j(\tau) \neq \beta_j(\tau')$ for some $\tau \neq \tau'$. This capability is essential when the covariates affect higher order moments or other distributional features of $Y \mid \mathbf{x}$. For instance, when analyzing education data (see Section 5), it is important not only to identify the factors that impact educational outcomes, but also to determine whether those effects are different for low-, medium, or high-achieving students. Such heterogeneous, quantile-specific effects can have far-reaching implications for policy interventions. In general, quantile regression provides a robust and comprehensive view of the relationship between covariates and the response variable, leading to many important applications: medicine (Kottas and Gelfand, 2001), finance (Bassett and Chen, 2002), and environmental studies (Pandey and Nguyen, 1999), among many others.

Broadly, there are several important components and considerations in quantile regression. First, quantile-specific linear coefficient *estimates* are obtained to detect potentially heterogeneous effects, $\beta_j(\tau) \neq \beta_j(\tau')$ for some $\tau \neq \tau'$, including both magnitude and direction. Second, quantile-specific *uncertainty quantification* provides important context for these coefficients and facilitates comparisons across both quantiles and variables. Third, when p is moderate or large, quantile-specific *subset selection* provides more parsimonious

summaries and identifies the most impactful covariates across the distribution $Y \mid \mathbf{x}$. Each of these targets must simultaneously respect the fundamental *smoothness* across quantiles: estimates, uncertainties, and selections should be similar for adjacent quantiles. Finally, the algorithms that deliver these results should be scalable in both the number of observations n and the number of covariates p .

The confluence of these demands creates a challenging environment for general statistical procedures. Existing approaches diverge into separate paradigms, each with their own limitations (see Sections 1.1 and 1.2). With this in mind, we seek to

1. Develop a decision analysis framework for quantile regression that is foundational, coherent, and compatible with any Bayesian regression model.

Our decision analysis integrates quantile regression into a data-centric Bayesian workflow that prioritizes suitable modeling of observed data, rather than adherence to certain quantile modeling requirements (see Sections 1.1 and 1.2). This broadens the utility of quantile regression, since it can be incorporated alongside traditional posterior summaries such as posterior means and credible intervals for model parameters. At the same time, the foundational and general nature of the decision analysis provides a new path to

2. Rigorously unify divergent approaches for Bayesian quantile regression.

From this perspective, the decision analysis provides essential context for comparing and contrasting the large array of existing Bayesian quantile regression models. More specifically, the inferential goal of the decision analysis is to

3. Deliver optimal (in a decision theory sense) point estimates and uncertainty quantification for conditional quantile functions and quantile-specific linear coefficients.

This goal is shared by many quantile regression approaches, and thus presents an opportunity for competitive evaluations (Section 4). More uniquely, via decision analysis we

4. Provide efficient algorithms for quantile-specific subset selection.

Subset selection is a daunting task—especially for quantile regression. Our decision analysis leverages state-of-the-art search algorithms and subset selection strategies for mean regression, and neatly adapts them to quantile regression.

Before expanding upon these goals and contributions, we first review existing Bayesian and frequentist methods for quantile regression—both to showcase the successes in this area and to highlight the need for methodological advances.

1.1 Separate Quantile Regressions

Separate quantile regression techniques estimate independent models for any set of quantiles, providing targeted estimation for each τ . Given paired data $\{(\mathbf{x}_i, y_i)\}_{i=1}^n$, [Koenker and Bassett Jr \(1978\)](#) introduced this approach from a frequentist perspective, obtaining quantile-specific coefficient estimates by minimizing the check loss

$$\hat{\boldsymbol{\beta}}(\tau) = \arg \min_{\boldsymbol{\beta}} \sum_{i=1}^n \rho_{\tau}\{y_i, \mathbf{x}_i^{\top} \boldsymbol{\beta}(\tau)\} \quad (2)$$

where $\rho_{\tau}(a, b) = \{a - b(\tau - \mathbb{1}_{a-b < 0})\}$. Since no closed-form solutions exist, (2) is usually solved by linear programming. However, the solutions are computed separately for each τ with no mechanism for information-sharing between $\hat{\boldsymbol{\beta}}(\tau)$ and $\hat{\boldsymbol{\beta}}(\tau')$ at nearby quantiles τ, τ' . As a result, the estimates can be erratic and non-smooth across τ , especially for extreme quantiles near zero or one. Confidence intervals are obtained through bootstrapping, which is computationally intensive, or asymptotic approximations, which can be inaccurate for small to moderate n ([Koenker et al., 2017](#)). Similar to point estimation, there is no information-sharing across quantiles for these interval estimates.

The Bayesian analog to (2) uses separate, quantile-specific asymmetric Laplace (AL) likelihoods for $\mathbf{y} = \{y_i\}_{i=1}^n$ given $\mathbf{X} = \{\mathbf{x}_i\}_{i=1}^n$ with centrality parameters $\{\mathbf{x}_i^{\top} \boldsymbol{\beta}(\tau)\}_{i=1}^n$ ([Yu](#)

and Moyeed, 2001):

$$p_{\tau}\{\mathbf{y} \mid \mathbf{X}, \boldsymbol{\beta}(\tau)\} = \prod_{i=1}^n \tau(1 - \tau) \exp[-\rho_{\tau}\{y_i, \mathbf{x}_i^{\top} \boldsymbol{\beta}(\tau)\}]. \quad (3)$$

Bayesian inference proceeds by placing priors on $\boldsymbol{\beta}(\tau)$ and inferring posterior distributions separately for each τ . Under a flat prior on $\boldsymbol{\beta}(\tau)$ and the likelihood (3), the maximum *a posteriori* estimator yields the same solution as (2). Broader theoretical justification is provided by Sriram et al. (2013), who detail sufficient conditions under which the posterior for $\boldsymbol{\beta}(\tau)$ is strongly consistent. Convenient parameter expansions have been developed to facilitate posterior sampling under (3) (Kozumi and Kobayashi, 2011; Fasiolo et al., 2021), which has led to widespread implementation with open source software (Benoit and Van den Poel, 2017; Alhamzawi and Ali, 2020).

In general, Bayesian quantile regression with the AL likelihood faces significant limitations. First, there is no information-sharing among nearby quantiles, which results in excessively large posterior uncertainties and underpowered inference for $\boldsymbol{\beta}(\tau)$, especially for extreme quantiles near zero or one (see Sections 4-5). Second, an AL likelihood must be specified for each τ , which induces distinct Bayesian models for the same data, typically with no attempt to reconcile or combine them. Finally, the AL likelihood often produces a substantially inadequate model for real data across many, if not all τ , which undermines the interpretability of the resulting inferences. Kowal and Wu (2024) proposed a transformation-based generalization of (3) to improve model adequacy, but did not address the previous two concerns.

1.2 Simultaneous Quantile Regression Methods

The lack of information-sharing across quantiles for separate (frequentist or Bayesian) quantile regression estimators commonly results in probabilistically incoherent quantile estimates. Specifically, separate quantile estimates often exhibit undesirable *quantile crossing*,

which occurs when $\mathbf{x}^\top \boldsymbol{\beta}(\tau) > \mathbf{x}^\top \boldsymbol{\beta}(\tau')$ for $\tau < \tau'$, violating basic probability properties for the implied conditional distribution of $Y \mid \mathbf{x}$. In response, a variety of Bayesian and frequentist methodologies have been developed to provide quantile regressions that ensure both smoothness and non-crossing of the coefficients across quantiles τ . In contrast to separate quantile regression methods, these *simultaneous* quantile regression methods fit a singular model to the data that estimates all quantiles of $Y \mid \mathbf{x}$.

Bondell et al. (2010) proposed to estimate linear quantiles (1) jointly across τ and subject to constraints that enforce quantile non-crossing. Kadane and Tokdar (2012) introduced a suitable Bayesian version. Alternative likelihoods to the AL (3) have included empirical likelihoods (Yang and He, 2012) and substitution likelihoods (Dunson and Taylor, 2005), which allow simultaneous inference for multiple quantiles. Other approaches estimate (1) by specifying semi- or non-parametric distributions for the errors $\{y_i - \mathbf{x}_i^\top \boldsymbol{\beta}(\tau)\}$ that satisfy certain quantile restrictions (Kottas and Gelfand, 2001; Kottas and Krnjajić, 2009; Reich et al., 2009; Reich and Smith, 2013). Taddy and Kottas (2010) specified a joint model for (Y, \mathbf{x}) and then inferred the conditional quantiles of $Y \mid \mathbf{x}$, which enforces quantile non-crossing but sacrifices a convenient form for $Q_\tau(Y \mid \mathbf{x})$ such as linearity (1).

A principal criticism of simultaneous quantile regression methods is their complexity, both for modelling and computing. For many semi- or non-parametric simultaneous methods, the functional form of the conditional quantiles deviates from the linear parameterization (1). Consequently, inference and comparisons among quantile-specific covariate effects are difficult to interpret and detection of heterogeneous covariate effects is more challenging. Further, models constrained to prevent quantile crossing require sophisticated optimization techniques or sampling algorithms, which present significant burdens for even moderately-sized data. Related, open source software for these methods is lacking. Finally, the modeling and computational complexity of these methods inhibits *quantile-specific subset selection*, which we discuss below.

1.3 Subset Selection in Quantile Regression

The goal of subset selection is to identify parsimonious representations of the regression function without sacrificing predictive power. This is particularly useful when p is moderate or large: with fewer active (or selected) covariates, it is easier to interpret the effects of each variable. Further, subset selection reduces storage requirements and can lower the variability of the estimated effects. For quantile regression, there is the added complexity that subset selection must be quantile-specific. This further aids in detecting covariate heterogeneity, as the subsets are allowed to vary between quantiles.

Among separate quantile regression methods, modifications to (2) have been developed for quantile-specific variable selection. Sparse estimates are obtained by appending a penalty term to (2), such as an ℓ_1 -penalty (Wu and Liu, 2009; Belloni and Chernozhukov, 2011; Wang et al., 2012; Lee et al., 2014). The sparsity among penalized quantile regression estimates is controlled by a tuning parameter, typically selected via cross-validation, which can be computationally intensive for the (penalized) objective (2). These methods do not provide uncertainty quantification and are limited in that common sparsity penalties i) introduce overshrinkage of nonzero effects and ii) severely restrict the subset search path. Critically, these methods focus on selecting a single “best” subset. However, even for moderate p with correlated covariates or weak signals, there are often many subsets that offer similar predictive accuracy. Thus, it can be misleading to report only a single “best” subset; consideration of a broader collection of “near-optimal” subsets can be more comprehensive and informative, but requires a robust subset search (Kowal, 2022).

Although frequentist subset search and selection is well-studied for mean regression (Furnival and Wilson, 2000; Hofmann et al., 2007; Bertsimas et al., 2016), extensions to quantile regression are so far unavailable.

For Bayesian variable selection with separate AL likelihoods (3), it is common to use sparsity or shrinkage priors for $\beta(\tau)$ (Li and Zhu, 2008; Alhamzawi et al., 2012; Chen

et al., 2013; Keil et al., 2020; Dao et al., 2022). However, these priors do not resolve the fundamental inadequacies of the AL model. Further, each of these methods selects variables marginally, either via posterior inclusion probabilities or credible intervals that exclude zero. Under the AL likelihood, marginal posteriors for $\beta_j(\tau)$ are often characterized by large uncertainty, which results in severely underpowered variable selection (see Section 4).

For simultaneous quantile regression methods, no obvious path toward quantile-specific subset selection emerges. These methods, already burdened by complex constraints or semi- or non-parametric specifications, are not well-suited to incorporate cardinality constraints for each quantile. Thus, we consider alternative approaches.

1.4 Overview of the Proposed Approach

To address the gaps in quantile regression methodology, we develop a Bayesian decision analysis for estimation, uncertainty quantification, and subset selection for quantile regression. Our methodology centers around first building a Bayesian model to capture salient features in the data, and then extracting targeted summaries of the *model-based* conditional quantiles. The general procedure is outlined in Algorithm 1.

Our formulation introduces several overarching advances to Bayesian quantile regression. First, the machinery is compatible with *any* Bayesian regression model \mathcal{M} for $Y \in \mathbb{R}$, including non-linear and non-parametric models (Pratola et al., 2020), Bayesian model averaging (Raftery et al., 1997), and Bayesian model stacking (Yao et al., 2018), among many others. Our framework remains compatible with separate Bayesian AL models and Bayesian simultaneous quantile regression models, thus offering a unified framework for these divergent approaches. However, the enhanced generality of our approach allows the Bayesian modeler to build \mathcal{M} to be suitable for the observed data, rather than to satisfy certain quantile-specific modeling requirements, such as AL likelihoods or unwieldy constraints.

Algorithm 1 Bayesian decision analysis for quantile regression

1. Fit a Bayesian regression model \mathcal{M} (e.g., (4))

Inputs: paired data $\{(\mathbf{x}_i, y_i)\}_{i=1}^n$

Output: posterior distribution (e.g., posterior samples) of the model-based conditional quantiles $\{Q_\tau(Y \mid \mathbf{x}_i, \boldsymbol{\theta})\}_{i=1}^n$ (e.g., (5)) for each quantile τ

2. Conduct Bayesian decision analysis for quantile regression:

- (a) Compute quantile-specific point estimates (Sections 2.1 and 2.4)

Output: *optimal actions* (e.g., (8)) that minimize the quantile-focused loss (7) for each quantile τ (nonlinear case: Section 2.4)

- (b) Provide quantile-specific posterior uncertainty quantification (Section 2.2)

Output: distribution for the *posterior action* (9) for each quantile τ

- (c) Search, filter, and select quantile-specific subsets (Section 3)

Output: quantile-specific *acceptable family* (17) that collects near-optimal subsets; quantile-specific *smallest acceptable subset* (18); and quantile-specific *variable importance* metrics (19).

Next, we design a decision analysis that extracts point estimates of quantile-specific coefficients from the model \mathcal{M} conditional quantile functions. Like any decision analysis, we must select a loss function; our approach features a *quantile-focused squared error loss*. This choice is motivated through its close connection with the Wasserstein distance between measures (Fréchet, 1948) and enables efficient, closed-form computation of optimal (in a decision analysis sense) coefficients for any quantile and any subset of predictors. Crucially, the model \mathcal{M} conveys regularization, both in the traditional sense (i.e., shrinkage of extraneous coefficients to zero) and via smoothness and information-sharing across nearby quantiles. Thus, while \mathcal{M} need not feature linear quantiles (1), the conditional quantiles under a singular model \mathcal{M} are probabilistically coherent and typically smooth across τ .

The underlying Bayesian regression model \mathcal{M} also delivers uncertainty quantification for the quantile-specific linear coefficients. In particular, the solution to each quantile-specific decision analysis is a posterior functional, which provides posterior inference for the linear quantile coefficients. We emphasize that this procedure derives from a single

model \mathcal{M} and does not lead to data re-use or model re-fitting for multiple quantiles.

Finally, we leverage the decision analysis framework to achieve quantile-specific subset search and selection. Our approach yields closed-form linear coefficient estimates for any quantile and any subset, and unlocks decision analysis strategies for variable selection previously deployed only for mean regression (Hahn and Carvalho, 2015; Woody et al., 2021; Kowal, 2021, 2022). We extend these approaches for quantile regression and design a subset search procedure to accumulate an *acceptable family* of subsets that provide strong predictive accuracy for each quantile. From this acceptable family, we recommend one subset based on the parsimony principle (i.e., the smallest subset in this family), but also construct variable importance metrics to avoid the overreliance on any single “best” subset. This is especially important when multiple subsets offer similar predictive accuracy. Our variable importance metrics seek to provide additional context in this common scenario.

The remainder of the paper is organized as follows. In Section 2, we introduce posterior decision analysis for quantile regression. Section 3 describes our quantile-specific subset search and selection procedure. We provide a simulation study in Section 4 to evaluate the proposed methodology for prediction, inference, selection, and quantile crossing. In Section 5 we conduct a quantile regression analysis using data on end-of-grade test scores for children in North Carolina. We conclude in Section 6. Supplementary materials include proofs to all results, Bayesian model specifications, additional simulation results, and an R package¹ implementing the proposed methodology.

2 Bayesian Decision Analysis for Quantile Regression

Our approach to quantile regression first constructs a Bayesian regression model to capture salient features of $Y \mid \mathbf{x}$. Then, we use Bayesian decision analysis to provide linear summaries of the model-based quantiles. Crucially, the user chooses the underlying

¹Codes implementing the proposed subset search and selection methodology are available at <https://github.com/jfeldman396/QRSubsets>

Bayesian model, which is unhindered by rigid structures imposed by models that require quantile-specific likelihoods (Section 1.1) or constraints (Section 1.2).

Given paired data $\{(\mathbf{x}_i, y_i)\}_{i=1}^n$, consider a Bayesian regression model \mathcal{M} for response variable $Y \in \mathbb{R}$ parameterized by $\boldsymbol{\theta}$. Consistent with a data-centric Bayesian workflow, suppose \mathcal{M} has been curated to best capture the conditional distribution of $Y \mid \mathbf{x}$, which may include nonlinearity, skewness, and heteroscedasticity, among many other features.

Importantly, \mathcal{M} implicitly models the quantiles of $Y \mid \mathbf{x}$. To see this, consider the class of additive location-scale models:

$$y_i = f(\mathbf{x}_i) + s(\mathbf{x}_i)\epsilon_i, \quad \epsilon_i \stackrel{iid}{\sim} F \quad (4)$$

where F is a cumulative distribution function (CDF) such that ϵ_i has mean zero and variance one. Under (4), the conditional quantile function for any τ and covariate value \mathbf{x} is a function of model parameters $\boldsymbol{\theta} = (f, s)$:

$$Q_\tau(Y \mid \mathbf{x}_i, \boldsymbol{\theta}) = f(\mathbf{x}_i) + s(\mathbf{x}_i)F^{-1}(\tau). \quad (5)$$

Given a prior $p(\boldsymbol{\theta})$, Bayesian inference for (4) targets the posterior distribution $p(\boldsymbol{\theta} \mid \mathbf{y})$. Then, for any τ , the model \mathcal{M} posterior propagates uncertainty to the conditional quantiles via (5). Accordingly, we view $Q_\tau(Y \mid \mathbf{x}, \boldsymbol{\theta})$ as a *posterior functional*. When the error quantile function F^{-1} is smooth in τ , then the implied model-based quantiles (5) inherit this smoothness. Assuming \mathcal{M} is a valid probability model for $Y \mid \mathbf{x}$, $Q_\tau(Y \mid \mathbf{x}_i, \boldsymbol{\theta})$ is guaranteed to avoid quantile crossing.

Leveraging the Bayesian model \mathcal{M} , our goal is to provide linear quantile estimates, uncertainty quantification, and subset selection. We design a *decision analysis* for each task. Central to this approach is a loss function $\mathcal{L}\{Q_\tau(Y \mid \mathbf{x}, \boldsymbol{\theta}), \mathbf{x}^\top \boldsymbol{\delta}_S(\tau)\}$ that evaluates the accuracy of a quantile-specific *linear action*, $\mathbf{x}^\top \boldsymbol{\delta}_S(\tau)$, with active (i.e., nonzero) coefficients

for a given subset $S \subseteq \{1, \dots, p\}$ of covariates. Nonlinear actions such as quantile-specific trees or additive functions are also compatible within this framework (see Section 2.4).

Since the model-based quantiles $Q_\tau(Y \mid \mathbf{x}, \boldsymbol{\theta})$ are unknown but inherit a posterior distribution under \mathcal{M} through $p(\boldsymbol{\theta} \mid \mathbf{y})$, the optimal coefficients are obtained by minimizing the posterior expected loss:

$$\hat{\boldsymbol{\delta}}_S(\tau) = \arg \min_{\boldsymbol{\delta}_S} E_{\boldsymbol{\theta} \mid \mathbf{y}} \mathcal{L}\{Q_\tau(Y \mid \mathbf{x}, \boldsymbol{\theta}), \mathbf{x}^\top \boldsymbol{\delta}_S(\tau)\}. \quad (6)$$

Thus, (6) provides linear quantile estimation, specific to each quantile τ and each subset S , under the model \mathcal{M} and the loss \mathcal{L} .

These steps—fitting a Bayesian model \mathcal{M} and then minimizing a posterior expected loss—are the foundational and uncontroversial components of a Bayesian decision analysis. The principal task is to specify the loss function \mathcal{L} . We propose a *quantile-focused squared error loss*, aggregated over the covariate values $\{\mathbf{x}_i\}_{i=1}^n$:

$$\mathcal{L}\{Q_\tau(Y \mid \mathbf{x}, \boldsymbol{\theta}), \mathbf{x}^\top \boldsymbol{\delta}_S(\tau)\} = \sum_{i=1}^n \|Q_\tau(Y_i \mid \mathbf{x}_i, \boldsymbol{\theta}) - \mathbf{x}_i^\top \boldsymbol{\delta}_S(\tau)\|_2^2. \quad (7)$$

The loss function (7) is exceptionally convenient for point estimation (Section 2.1), uncertainty quantification (Section 2.2), and subset selection (Section 3), with closed-form estimation and efficient subset search strategies. More formally, we establish deeper theoretical justification for (7) via connections to Wasserstein-based density regression (Section 2.3).

2.1 Point Estimation for Linear Quantiles

A significant advantage of using the quantile-focused squared error loss (7) is in the availability of a closed-form solution for (6). For any quantile τ and subset of covariates S , we derive the optimal linear action:

Lemma 2.1. *Suppose $E_{\boldsymbol{\theta} \mid \mathbf{y}} \|Q_\tau(Y_i \mid \mathbf{x}_i, \boldsymbol{\theta})\|_2^2 < \infty$ for $i = 1, \dots, n$. For any quantile*

$\tau \in (0, 1)$ and any subset of predictors $S \subseteq \{1, \dots, p\}$, the optimal action (6) under the quantile-focused squared error loss (7) is

$$\hat{\boldsymbol{\delta}}_S(\tau) = (\mathbf{X}_S^\top \mathbf{X}_S)^{-1} \mathbf{X}_S^\top \hat{\mathbf{Q}}_\tau(\mathbf{X}) \quad (8)$$

with zeros for indices $j \notin S$, where \mathbf{X}_S is the $n \times |S|$ matrix of active covariates for subset S , $\hat{\mathbf{Q}}_\tau(\mathbf{X}) = \{\hat{Q}_\tau(\mathbf{x}_1), \dots, \hat{Q}_\tau(\mathbf{x}_n)\}^\top$, and $\hat{Q}_\tau(\mathbf{x}_i) = E_{\boldsymbol{\theta}|\mathbf{y}}\{Q_\tau(Y_i | \mathbf{x}_i, \boldsymbol{\theta})\}$.

The optimal linear action under the quantile-focused squared error loss is the least squares solution with response vector $\hat{\mathbf{Q}}_\tau(\mathbf{X})$ and covariate submatrix \mathbf{X}_S . The result is a linear point estimate of the τ th conditional quantile of $Y | \mathbf{x}$, which provides the magnitude and direction of the relationship between each covariate and a specific percentile of the response. These coefficients may also be used for quantile-specific prediction.

In general, the posterior expected conditional quantiles $\hat{Q}_\tau(\mathbf{x}_i) = E_{\boldsymbol{\theta}|\mathbf{y}}\{Q_\tau(Y_i | \mathbf{x}_i, \boldsymbol{\theta})\}$ under \mathcal{M} are not available in closed-form. Monte Carlo approximations are easily obtained via $E_{\boldsymbol{\theta}|\mathbf{y}}[Q_\tau(Y_i | \mathbf{x}_i, \boldsymbol{\theta})] \approx M^{-1} \sum_{m=1}^M Q_\tau(Y_i | \mathbf{x}_i, \boldsymbol{\theta}^m)$ where $\{\boldsymbol{\theta}^m\}_{m=1}^M \sim p(\boldsymbol{\theta} | \mathbf{y})$.

It is apparent from Lemma 2.1 that different models will provide different optimal linear actions (6), since $\hat{\mathbf{Q}}_\tau(\mathbf{X})$ will vary from model to model. An important special case emerges for homoscedastic linear regression:

Corollary 1. *For the location-scale model (4) with linearity $f(\mathbf{x}_i) = \mathbf{x}_i^\top \boldsymbol{\beta}(\tau)$, homoscedasticity $s(\mathbf{x}_i) = \sigma$, and an intercept $x_{i1} = 1$, the optimal action (6) under (7) for the full set of covariates is $\hat{\boldsymbol{\delta}}_{\{1, \dots, p\}}(\tau) = [\hat{\beta}_1(\tau), \{\hat{\beta}_j\}_{j=2}^p]$ for any τ , where $\hat{\beta}_1(\tau) = E_{\boldsymbol{\theta}|\mathbf{y}}[\beta_1 + \sigma F^{-1}(\tau)]$ and $\hat{\beta}_j = E_{\boldsymbol{\theta}|\mathbf{y}}\beta_j$ for $j = 2, \dots, p$.*

For homoscedastic linear regression, the quantile-specific linear action for the full set of covariates $S = \{1, \dots, p\}$ is precisely the posterior expectation of the linear model coefficients, with a quantile-specific shift for the intercept. This result also emphasizes the inability of homoscedastic linear regression to detect heterogeneous covariate effects;

excluding the intercept, the quantile-specific linear coefficients are constant across τ .

Alternatively, consider any Bayesian model \mathcal{M} with linear quantiles (1). Prominent examples include separate Bayesian AL regressions along with several simultaneous quantile methods (Section 1.2). In this case, the optimal action (6) under (7) with all covariates $S = \{1, \dots, p\}$ is the posterior expectation of the quantile-specific linear regression coefficients:

Corollary 2. *For any Bayesian model with linear quantiles $Q_\tau(Y_i | \mathbf{x}_i, \boldsymbol{\theta}) = \mathbf{x}_i^\top \boldsymbol{\beta}(\tau)$, the optimal action (6) under (7) for the full set of covariates is $\hat{\boldsymbol{\delta}}_{\{1, \dots, p\}}(\tau) = \hat{\boldsymbol{\beta}}(\tau)$, where $\hat{\boldsymbol{\beta}}(\tau) = E_{\boldsymbol{\theta}|\mathbf{y}} \boldsymbol{\beta}(\tau)$.*

Corollaries 1 and 2 show that, under common (mean and quantile) linear regression models, the optimal actions (6) are directly related to the posterior expectations of the regression coefficients. Thus, the point estimates (6) inherit regularization (shrinkage, sparsity, smoothness, etc.) from \mathcal{M} , which improves estimation, especially for large p .

While Corollaries 1 and 2 confirm reasonable behavior for the optimal action (6) under linear regression models, we emphasize the utility of Lemma 2.1 for quantile regression estimation under *any* Bayesian regression model. In particular, the analyst can prioritize curation of \mathcal{M} to capture complex features of the entire conditional distribution $Y | \mathbf{x}$, including nonlinearity, skewness, and heteroscedasticity, while (8) provides the optimal linear approximation of the model-based quantiles under the quantile-focused loss (7).

2.2 Posterior Uncertainty Quantification

To enable posterior uncertainty quantification for the quantile-specific linear coefficients, we revisit (6), but *without* the posterior expectation. Using the quantile-focused squared

error loss (7), we define the quantile-specific *posterior action* as the solution to

$$\begin{aligned}\boldsymbol{\delta}_S(\boldsymbol{\theta}; \tau) &= \arg \min_{\boldsymbol{\delta}_{S(\tau)}} \sum_{i=1}^n \|Q_\tau(Y_i \mid \mathbf{x}_i, \boldsymbol{\theta}) - \mathbf{x}_i^\top \boldsymbol{\delta}_S(\tau)\|_2^2 \\ &= (\mathbf{X}_S^\top \mathbf{X}_S)^{-1} \mathbf{X}_S^\top \mathbf{Q}_\tau(\mathbf{Y} \mid \mathbf{X}, \boldsymbol{\theta})\end{aligned}\tag{9}$$

for any subset of covariates S and any quantile τ , where $\mathbf{Q}_\tau(\mathbf{Y} \mid \mathbf{X}, \boldsymbol{\theta}) = \{Q_\tau(y_1 \mid \mathbf{x}_1, \boldsymbol{\theta}), \dots, Q_\tau(y_n \mid \mathbf{x}_n, \boldsymbol{\theta})\}^\top$. By design, (9) projects the posterior functional $\mathbf{Q}_\tau(\mathbf{Y} \mid \mathbf{X}, \boldsymbol{\theta})$ onto the corresponding sub-matrix of covariates, so $\boldsymbol{\delta}_S(\boldsymbol{\theta}; \tau)$ inherits a posterior distribution under \mathcal{M} .

Similar to the optimal action (6), the posterior action (9) can be linked directly to the model \mathcal{M} parameters by considering linear (mean or quantile) regression models. For homoscedastic linear regression, the posterior action returns the posterior distribution of the linear regression coefficients, with a quantile-specific shift for the intercept:

Corollary 3. *For the location-scale model (4) with linearity $f(\mathbf{x}_i) = \mathbf{x}_i^\top \boldsymbol{\beta}(\tau)$, homoscedasticity $s(\mathbf{x}_i) = \sigma$, and an intercept $x_{i1} = 1$, the posterior action (9) for the full set of covariates $S = \{1, \dots, p\}$ satisfies*

$$\boldsymbol{\delta}_{\{1, \dots, p\}}(\boldsymbol{\theta}; \tau) \sim p(\boldsymbol{\theta}^* \mid \mathbf{y})$$

where $\boldsymbol{\theta}^* = [\beta_1 + \sigma F^{-1}(\tau), \{\beta_j\}_{j=2}^p]$.

As in Corollary 2, a similar result is available when \mathcal{M} features linear quantiles (1): the posterior action for the full set of covariates is distributed according to the posterior distribution of the quantile-specific regression coefficients $\boldsymbol{\beta}(\tau)$.

Once again, the advantage of the posterior action (9) is that it delivers quantile- and subset-specific uncertainty quantification under *any* Bayesian model \mathcal{M} . Crucially, the posterior action does not require Bayesian model re-fitting for each choice of quantile τ or

subset S : all uncertainty derives from the single model \mathcal{M} posterior. The distribution of (9) is easily accessed given posterior samples $\{\boldsymbol{\theta}^m\}_{m=1}^M$: we simply compute $Q_\tau(Y \mid \mathbf{X}, \boldsymbol{\theta}^m)$ and plug the result into (9) for any identified subset S .

2.3 Connection with the Wasserstein Geometry

The quantile-focused squared error loss (7) is motivated through its connection with the Wasserstein geometry on the space of probability measures. Consider a posterior decision analysis for point-estimation of the probability density function (PDF) of $Y \mid \mathbf{x}$ under \mathcal{M} . Density regression can be accomplished under Wasserstein geometry, which defines valid metrics over the space of random probability measures (Petersen et al., 2021). Formally, let \mathcal{D} be the space of univariate PDFs with finite second moments and consider the random PDF $g \in \mathcal{D}$ for $Y \mid \mathbf{x}$ with associated (conditional) CDF G and quantile function G^{-1} . Regression of g on covariates \mathbf{x} finds $h \in \mathcal{D}$ (with CDF H and quantile function H^{-1}) that minimizes the expected squared-Wasserstein distance

$$h^*(\mathbf{x}) = \operatorname{argmin}_{h \in \mathcal{D}} E_{g \mid \mathbf{x}} d_W^2(g, h). \quad (10)$$

Equivalently, (10) minimizes the expected L^2 distance between conditional (on \mathbf{x}) quantiles G^{-1} and H^{-1} integrated over all τ :

$$h^*(\mathbf{x}) = \operatorname{argmin}_{h \in \mathcal{D}} E_{g \mid \mathbf{x}} \int_0^1 \|G_\tau^{-1} - H_\tau^{-1}\|_2^2 d\tau. \quad (11)$$

Classically, data-driven estimation of (11) requires multiple realizations from $Y_i \mid \mathbf{x}_i$ for each covariate value \mathbf{x}_i in order to compute empirical quantiles $\hat{G}_\tau^{-1}(Y_i \mid \mathbf{x}_i)$. By computing these empirical quantiles over a fine grid $\tau \in \{0 < \tau_1, \dots, \tau_\ell < 1\}$, Petersen et al. (2021) proposed

to estimate (11) by minimizing

$$\sum_{\tau=\tau_1}^{\tau_\ell} \sum_{i=1}^n \|\hat{G}_\tau^{-1}(Y_i | \mathbf{x}_i) - H_\tau^{-1}(Y_i | \mathbf{x}_i)\|_2^2. \quad (12)$$

over densities $h \in \mathcal{D}$, and showed that the solution is a consistent estimator of h^* .

For Bayesian decision analysis, the analogous approach is to replace the empirical quantiles $\hat{G}_\tau^{-1}(Y_i | \mathbf{x}_i)$ by the model \mathcal{M} quantiles $Q_\tau(Y_i | \mathbf{x}_i, \boldsymbol{\theta})$. Unlike the empirical quantiles, the model-based quantiles do *not* require multiple realizations of $Y_i | \mathbf{x}_i$ at each \mathbf{x}_i . Then, like in (6), we minimize the posterior expected loss

$$E_{\boldsymbol{\theta}|\mathbf{y}} \sum_{\tau=\tau_1}^{\tau_\ell} \sum_{i=1}^n \|Q_\tau(Y_i | \mathbf{x}_i, \boldsymbol{\theta}) - \boldsymbol{\delta}(\mathbf{x}_i; \tau)\|_2^2 \quad (13)$$

over densities with corresponding quantile functions $\boldsymbol{\delta}(\mathbf{x}_i; \tau)$. Thus, the minimizer of (13) is a model-based point estimate of the PDF (or quantile function) of $Y | \mathbf{x}$ under squared-Wasserstein loss.

To establish a connection with the proposed decision analysis for quantile regression in (6)-(7), we emphasize two critical choices for (13). First, we require linearity of the quantile function, $\boldsymbol{\delta}_S(\mathbf{x}; \tau) = \mathbf{x}^\top \boldsymbol{\delta}_S(\tau)$, possibly with a subset of active covariates $S \subseteq \{1, \dots, p\}$. This requirement aligns with our goals of linear quantile regression (1) and quantile-specific subset search and selection (Section 3). Second, the decision analysis in (6)-(7) elects *not* to impose the requirement that the estimated quantiles $\mathbf{x}^\top \boldsymbol{\delta}_S(\tau)$, taken jointly across τ , yield a valid density function for each \mathbf{x} . The primary motivation is tractability—including for point estimation, uncertainty quantification, and subset selection. Then, the collection of quantile-specific estimates $\hat{\boldsymbol{\delta}}_S(\tau)$ from (6)-(8), taken across $\tau \in \{\tau_1, \dots, \tau_\ell\}$, minimizes a modified version of the posterior expected squared-Wasserstein loss (13):

Lemma 2.2. *Let $\boldsymbol{\delta}(\mathbf{x}; \tau) = \mathbf{x}^\top \boldsymbol{\delta}_S(\tau)$ for any \mathbf{x} and any subset S of covariates. Then the minimizer of (13), without a density restriction, is given by the quantile estimators*

$\hat{\delta}(\mathbf{x}; \tau_m) = \mathbf{x}^\top \hat{\delta}_S(\tau_m)$ with $\hat{\delta}_S(\tau_m)$ computed from (8) separately for each $m = 1, \dots, \ell$.

This result provides additional motivation for the quantile-focused squared error loss (7), which is linked to Bayesian decision analysis for density estimation of $Y \mid \mathbf{x}$ under squared-Wasserstein loss.

We emphasize that the relaxation of the density requirement maintains alignment with our primary goals: estimation, uncertainty quantification, and selection of quantile-specific regression coefficients. We do not claim to provide valid density estimates. We do, however, observe that the estimated quantiles tend to preserve probabilistic coherence, such as quantile non-crossing (see Section E.5 of the supplementary material). Furthermore, this relaxation does not affect the validity of the proposed decision analysis: we specify a carefully-chosen loss function and minimize the posterior expected loss under the model \mathcal{M} . Indeed, quantile regression often focuses on a few select quantiles τ , such as upper or lower extremes, quartiles, and medians. Consideration of a fine grid $\tau \in \{\tau_1, \dots, \tau_\ell\}$, while feasible with the proposed approach, may offer little additional information.

2.4 Extensions for Nonlinear Quantiles

The proposed decision analysis framework for quantile estimation and uncertainty quantification is readily modified for nonlinear quantiles. First, recall that the Bayesian model \mathcal{M} is generic, and may or may not specify linear quantiles as in (1). For example, the additive location-scale model (4) may incorporate a nonlinear mean function $f(\mathbf{x})$ or scale function $s(\mathbf{x})$, each of which induces nonlinear quantiles via (5). In this case, the linear summaries from Sections 2.1-2.2 may not be suitable. Instead, the quantile-specific action $\delta_S(\mathbf{x}; \tau)$ (e.g., as in (13)) may be parametrized using decision trees or additive functions of \mathbf{x} , akin to Woody et al. (2021) for mean regression. Crucially, this does not completely sacrifice the computational convenience of our decision analysis: extending Lemma 2.1, the optimal action (similar to (6)) is still obtained by minimizing a least squares objective with

response vector $\hat{\mathbf{Q}}_\tau(\mathbf{X})$. Similar extensions are available for the posterior action (akin to (9)) to provide uncertainty quantification. However, nonlinear quantiles are not without drawbacks: they are typically more difficult to interpret, less amenable to subset selection, and require a choice for the parametrization of $\boldsymbol{\delta}_S(\mathbf{x}; \tau)$. Thus, we focus on linear quantile regression.

3 Quantile-Specific Subset Search and Selection

A primary benefit of the quantile-focused squared error loss is that for any τ and subset S of covariates, the optimal linear action is given by the least squares solution with covariate matrix \mathbf{X}_S and pseudo-response vector $\hat{\mathbf{Q}}_\tau(\mathbf{X})$. We leverage this result (Lemma 2.1) to provide new and efficient strategies for quantile-specific subset search and selection.

3.1 Subset Search with Decision Analysis

Subset search requires i) evaluation criteria to compare among subsets and ii) algorithms to efficiently explore the (typically massive) space of all 2^p subsets. For any quantile τ and subset S , we evaluate the optimal action $\hat{\boldsymbol{\delta}}_S(\tau)$ from (8) using two quantities. First,

$$L_S(\tau) = E_{\boldsymbol{\theta}|\mathbf{y}} \sum_{i=1}^n \|Q_\tau(Y_i | \mathbf{x}_i, \boldsymbol{\theta}) - \mathbf{x}_i^\top \hat{\boldsymbol{\delta}}_S(\tau)\|_2^2 \quad (14)$$

is the minimum achieved for each subset S and quantile τ under the quantile-focused squared error loss (7). Thus, (14) is a single number summary that compares the quantile estimates under the optimal action to the model-based conditional quantiles. Second, we compute

$$L_S(\boldsymbol{\theta}; \tau) = \sum_{i=1}^n \|Q_\tau(Y_i | \mathbf{x}_i, \boldsymbol{\theta}) - \mathbf{x}_i^\top \hat{\boldsymbol{\delta}}_S(\tau)\|_2^2, \quad (15)$$

which resembles (14) but instead inherits a posterior distribution via $p(\boldsymbol{\theta} | \mathbf{y})$ under model \mathcal{M} . Thus, (15) enables uncertainty quantification for the performance of each subset. The

evaluation criteria in (14) and (15) are used in conjunction to search and subsequently filter to the "near-optimal" or *acceptable* family of subsets (Kowal, 2021), specific to each quantile τ .

A key observation is that $L_{S_1}(\tau) - L_{S_2}(\tau) = \hat{L}_{S_1}(\tau) - \hat{L}_{S_2}(\tau)$, where $\hat{L}_S(\tau) = \sum_{i=1}^n \|\hat{Q}_\tau(\mathbf{x}_i) - \mathbf{x}_i^\top \hat{\boldsymbol{\delta}}_S(\tau)\|_2^2$, so we need only consider the residual sum-of-squares (RSS) $\hat{L}_S(\tau)$ from a linear predictor with response $\hat{Q}_\tau(\mathbf{x}_i) = E_{\boldsymbol{\theta}|\mathbf{y}}\{Q_\tau(Y_i | \mathbf{x}_i, \boldsymbol{\theta})\}$. Notably, classical and state-of-the-art subset search algorithms for mean regression rely on RSS comparisons among subsets (Furnival and Wilson, 2000; Hofmann et al., 2007; Bertsimas et al., 2016). Thus, our deployment of the quantile-focused squared error loss (14) enables adaptation of these strategies for quantile-specific subset search and selection.

When the complete enumeration of all possible 2^p subsets is not feasible, we apply the branch-and-bound (BBA) search algorithm (Furnival and Wilson, 2000) to efficiently eliminate non-competitive subsets. BBA uses a tree-based enumeration of all possible subsets to extract the most promising $m_k \leq \binom{p}{k}$ subsets for each size $k \in \{1, \dots, p\}$ according to RSS, which in our setting is equivalent to (14). A key benefit of BBA is that it provides a large number of candidate subsets m_k of each size k . Thus, we apply BBA as a pre-screening procedure to obtain *candidate subsets* $\mathbb{S}(\tau)$ for each quantile τ .

The inputs for the BBA algorithm are i) the model-based fitted quantiles $\{\hat{Q}_\tau(\mathbf{x}_i)\}$, ii) the covariates $\{\mathbf{x}_i\}$, and iii) the maximum number of subsets m_k to return for each subset size k , which should be chosen as large as computationally feasible. In our simulation and application, we set $m_k = 50$. An efficient implementation of the BBA algorithm is available in the `leaps` package in R, which provides fast filtering for $p \leq 35$; see the Section D of the supplement for details on our model-assisted pre-screening approach when $p > 35$.

3.2 Subset Filtration

Although it is tempting to consider subset *selection* based on $L_S(\tau)$, the well-known ordering properties of RSS apply in the current setting: for nested subsets $S_1 \subseteq S_2$, it is guaranteed that $L_{S_1}(\tau) \geq L_{S_2}(\tau)$. Thus, selection based on (14) alone will invariably and trivially select the full set of covariates, $S = \{1, \dots, p\}$. This motivates our consideration of $L_S(\boldsymbol{\theta}; \tau)$ in (15), which provides an alternative path for subset selection.

We compare the posterior loss (15) between any given subset, $L_S(\boldsymbol{\theta}; \tau)$, and the model-based fitted quantiles, $L_{\hat{Q}}(\boldsymbol{\theta}; \tau) = \sum_{i=1}^n \|Q_\tau(Y_i | \mathbf{x}_i, \boldsymbol{\theta}) - \hat{Q}_\tau(\mathbf{x}_i)\|_2^2$, which provide a useful and competitive benchmark. Specifically, we compute the percent increase in loss between the optimal linear action and the model-based fitted quantiles:

$$D_S(\tau) = 100 \times \{L_S(\boldsymbol{\theta}; \tau) - L_{\hat{Q}}(\boldsymbol{\theta}; \tau)\} / L_{\hat{Q}}(\boldsymbol{\theta}; \tau). \quad (16)$$

Crucially, $D_S(\tau)$ inherits a posterior distribution under \mathcal{M} , and is easily computed for each candidate subset $S \in \mathbb{S}(\tau)$ using posterior samples of $\boldsymbol{\theta}$. Then, from (16) we collect the subsets for which the optimal linear action has nonnegligible probability $\varepsilon > 0$ (under \mathcal{M}) of matching the performance of the fitted quantiles:

$$\mathbb{A}_\varepsilon(\tau) = \{S \in \mathbb{S}^\tau : p\{D_S(\tau) \leq 0 \mid \mathbf{y}\} \geq \varepsilon\}. \quad (17)$$

We refer to $\mathbb{A}_\varepsilon(\tau)$ as the *quantile-specific acceptable family*, which extends the acceptable family from mean regression to quantile regression (Kowal, 2021, 2022). Equivalently, $S \in \mathbb{A}_\varepsilon(\tau)$ if and only if there is a lower $(1 - \varepsilon)$ credible interval for $D_S(\tau)$ that includes zero (Kowal, 2021). Given this correspondence, we set $\varepsilon = 0.05$ by default.

Within the acceptable family, we select a subset based on the parsimony principle:

$$S_{small}(\tau) = \operatorname{argmin}_{S \in \mathbb{A}_\varepsilon(\tau)} |S| \quad (18)$$

which is the quantile-specific *smallest acceptable subset*. By construction, $S_{small}(\tau)$ reports the simplest (most parsimonious) explanation that maintains competitive estimation for the τ th quantile. The selected subset is quantile-specific, and thus it is informative to compare $S_{small}(\tau)$ across quantiles τ .

When (18) is nonunique, we select the subset that minimizes (14). In some cases, $A_\varepsilon(\tau)$ may be empty and $S_{small}(\tau)$ will be undefined, such as when the quantiles are highly nonlinear in \mathbf{x} . This outcome is informative: it suggests that the linear actions (6) are inadequate for the τ th quantile and must be replaced by alternative quantile summaries, such as trees or additive functions.

3.3 Quantifying Variable Importance

A principal advantage of curating the quantile-specific acceptable family (17) is that it contains more information than any single ("best") subset. In the common applied setting with moderate p , correlated covariates, or weak signals, there are typically many subsets that offer similar accuracy. Thus, we de-emphasize the selection of a single "best" subset and instead provide more comprehensive summaries of the quantile-specific acceptable family.

For each covariate j , we introduce a quantile-specific *variable importance* metric:

$$VI_j(\tau) = |A_\varepsilon(\tau)|^{-1} \sum_{S \in A_\varepsilon(\tau)} \mathbb{I}\{j \in S\} \quad (19)$$

which reports the proportion of acceptable subsets that include variable j . Informally, (19) measures how essential the j th covariate is for linearly predicting the τ th quantile. We are particularly interested in *keystone covariates* that appear in nearly all acceptable subsets, $VI_j(\tau) > q$ for some large cutoff $q \in [0, 1]$. Alternatively, while a variable j may be omitted from the "best" subset or $S_{small}(\tau)$, observing $VI_j(\tau) > 0$ implies that variable j belongs to at least one subset with near-optimal quantile prediction. Naturally, $VI_j(\tau)$ may vary with

τ , which implies that the importance of covariate j is heterogeneous across the percentiles of $Y \mid \mathbf{x}$.

4 Simulation Study

4.1 Simulation Design

We design a simulation study to compare the proposed methodology with competing methods for quantile regression. Response variables are simulated from the linear location-scale model

$$y_i = \mathbf{x}_i^\top \boldsymbol{\xi}^* + (\mathbf{x}_i^\top \boldsymbol{\gamma}^*) \epsilon_i, \quad \epsilon_i \stackrel{iid}{\sim} N(0, 1). \quad (20)$$

By design, (20) yields linear conditional quantile functions $Q_\tau^*(\mathbf{x}) = \mathbf{x}^\top \boldsymbol{\beta}^*(\tau)$, where $\beta_1^*(\tau) = 2 + \Phi^{-1}(\tau)$ and $\beta_j^*(\tau) = \xi_j^* + \Phi^{-1}(\tau)\gamma_j^*$, $j = 2, \dots, p$, with Φ the standard normal CDF. The covariate values \mathbf{x}_i are simulated independently for $i = 1, \dots, n$ from a Gaussian copula with uniform marginals and copula correlation $\rho_{\ell j} = 0.5^{|\ell-j|}$, which provides varying degrees of correlation among the predictors. Additional simulations with independent covariates ($\rho_{\ell j} = 0$) are available in Section E.2 of the supplement.

We enforce both sparsity and heterogeneous effects in the response distribution through $\boldsymbol{\xi}^*$ and $\boldsymbol{\gamma}^*$. First, we incorporate homogeneous quantile effects by setting $\xi_j^* = 2$ and $\gamma_j^* = 0$ for a pre-specified set of indices $j \in \text{hom} \subseteq \{2, \dots, p\}$, so the linear quantile coefficients for these variables satisfy $\beta_j^*(\tau) = 2$ for all τ . The intercepts are $\xi_1^* = 2$ and $\gamma_1^* = 1$. Next, for one covariate $\text{het} \in \{2, \dots, p\} \setminus \text{hom}$, we set $\gamma_{\text{het}}^* = h$ and $\xi_{\text{het}}^* = 0$, where, h controls the strength of the heteroscedasticity in (20) and thus the magnitude of $\beta_{\text{het}}^*(\tau) = \Phi^{-1}(\tau)h$. We determine h by selecting a heterogeneity ratio, $\text{HetRatio} = \text{var}(\mathbf{x}_i^\top \boldsymbol{\xi}^*)/\gamma_{\text{het}}^*$, from $\{0.5, 1\}$ for weak or strong heterogeneity, respectively. The remaining coefficients are fixed at zero.

To determine hom and het for p -dimensional (correlated) covariates, we isolate every fourth index using the sequence $\mathbf{I} = \{2 + 4j, j \in (0, \dots, \lfloor p/4 \rfloor)\}$ and let $\text{hom} = \{\mathbf{I} \setminus$

$\text{median}(\mathbf{I})\}$ and $het = \lfloor \text{median}(\mathbf{I}) \rfloor$. Given the dependence among the covariates, this ensures that the covariate with heterogeneous effects is at least moderately correlated with the remaining covariates, which is challenging for selection. A representation of this scheme is given below for $p = 10$, $\mathbf{I} = \{2, 6, 10\}$, $het = 6$, $hom = \{2, 10\}$:

$$\begin{aligned}\boldsymbol{\gamma}^* &= (\gamma_1^* = 1, \underbrace{\gamma_2^* = 0, \dots, \gamma_6^* = h}_{hom}, \dots, \underbrace{\gamma_{10}^* = 0}_{hom}) \\ \boldsymbol{\xi}^* &= (\xi_1^* = 2, \underbrace{\xi_2^* = 2, \dots, \xi_6^* = 0}_{het}, \dots, \underbrace{\xi_{10}^* = 2}_{hom}).\end{aligned}$$

We carry out our simulation design for $(n, p) \in \{(500, 20), (200, 50), (100, 100)\}$ and $\text{HetRatio} \in \{0.5, 1\}$ across 50 independent repetitions of the data generating process in each setting. For brevity and because they more closely mirror our application, we present and discuss results for the $(n, p) \in \{(500, 20), (200, 50)\}$ settings. However, the $n = 100, p = 100$ results were qualitatively similar, and Section E of the supplement reports the results for all outstanding settings with nearly identical conclusions.

For the Bayesian model \mathcal{M} , we fit a linear location-log scale (LL-LS) regression model to our simulated data:

$$y_i \mid \boldsymbol{\theta} \stackrel{indep}{\sim} \text{Normal}[\mathbf{x}_i^\top \boldsymbol{\xi}, \{\sigma \exp(\mathbf{x}_i^\top \boldsymbol{\gamma})\}^2] \quad (21)$$

with model parameters $\boldsymbol{\theta} = (\sigma, \boldsymbol{\xi}, \boldsymbol{\gamma})$. By design, both the mean and variance functions are misspecified under \mathcal{M} : both include all covariates, even those with true null effects, while the variance function is nonlinear. The full Bayesian specification of \mathcal{M} is available in Section C of the supplement, but we note here that regularizing priors are specified on both $\boldsymbol{\xi}$ and $\boldsymbol{\gamma}$ and the model is estimated using **STAN** (Carpenter et al., 2017). Posterior samples of the τ th conditional quantile function under \mathcal{M} are easily computed under (21): for each posterior sample $\boldsymbol{\theta}^s$ and any covariate value \mathbf{x} , we simply compute $Q_\tau(Y \mid \mathbf{x}, \boldsymbol{\theta}^s) =$

$$\mathbf{x}^\top \boldsymbol{\xi}^s + \sigma^s \exp(\mathbf{x}^\top \boldsymbol{\gamma}^s) \Phi^{-1}(\tau).$$

Under each $(n, p, \text{HetRatio})$ combination, we curate acceptable families for $\tau \in \{0.01, 0.05, 0.25, 0.5, 0.75, 0.95, 0.99\}$ using the proposed methodology in Sections 2-3 under default settings ($m_k = 50, \varepsilon = 0.05$). Among the subsets in each $\mathbb{A}_{0.05}(\tau)$, we evaluate quantile prediction, inference, and variable selection for $S_{\text{small}}(\tau)$.

For a frequentist competitor, we fit adaptive LASSO quantile regressions separately for each τ , which use an ℓ_1 -penalized check loss for sparse estimation (Wu and Liu, 2009). The (sparsity) tuning parameter is selected by 5-fold cross-validation with the one-standard-error rule (aLASSO), and an efficient implementation is available in the R package `rqPen` (Sherwood and Maidman, 2017).

For a Bayesian competitor, we fit Bayesian linear quantile regressions with the AL likelihood and adaptive LASSO priors (AL_{Bayes} ; Alhamzawi et al. (2012)) using default settings in the `bayesQR` package in R (Benoit and Van den Poel, 2017). Point estimates are computed using posterior means of the coefficients. Variable selection with AL_{Bayes} identifies those covariates for which the 95% highest posterior density intervals for the coefficients do not include zero.

Finally, we compare to the quantile estimates from the model-based fitted quantiles $\hat{\mathbf{Q}}(\mathbf{X})$ under (21) (\mathbf{Q}_{hat}). This competitor does not provide *linear* coefficient estimates, uncertainty quantification, or selection. Nonetheless, it is a useful benchmark to evaluate whether our linear quantile estimators sacrifice any predictive performance relative to an unrestricted estimator under \mathcal{M} . Posterior inference for both \mathcal{M} and AL_{Bayes} is based on 2500 posterior samples accumulated after a burn-in of 2500.

4.2 Quantile Prediction

We first summarise the predictive performance of the competing methods on hold-out datasets $(\mathbf{X}_{\text{test}}, \mathbf{y}_{\text{test}})$ with $n_{\text{test}} = 1000$, which are generated independently and identi-

cally distributed to the training data. We compute out-of-sample quantile predictions, say $\tilde{Q}_\tau(\mathbf{X}_{test})$, for each competitor. For each τ , we evaluate the performance using three metrics: i) the mean-squared error (MSE) between the ground-truth $Q_\tau^*(\mathbf{X}_{test})$ and predictions $\tilde{Q}_\tau(\mathbf{X}_{test})$, ii) the average check loss between \mathbf{y}_{test} and $\tilde{Q}_\tau(\mathbf{X}_{test})$, and iii) the calibration of $\tilde{Q}(\mathbf{X}_{test})$ computed via $n_{test}^{-1} \sum_{i=1}^{n_{test}} \mathbb{1}\{y_{test_i} \leq \tilde{Q}_\tau(\mathbf{x}_{test_i})\}$, which should be near τ for a well-calibrated quantile estimator (Section E.5 of the supplementary material). The results for MSE and check loss for $\tau \in \{0.01, 0.5, 0.99\}$ and $n = 200, p = 50, \text{HetRatio} = 1$ across simulations are presented in Figure 1; results for other simulation settings are qualitatively similar, see Section E of the supplement.

Across all quantiles, the proposed approach demonstrates exceptional quantile prediction. The quantile MSEs for $S_{small}(\tau)$ are significantly lower than those for competing frequentist and Bayesian methods, especially for extreme quantiles near zero or one. $S_{small}(\tau)$ decisively outperforms aLASSO in check loss, even though aLASSO—unlike $S_{small}(\tau)$ —directly optimizes (penalized) check loss via (2). Finally, the linear quantile predictions from $S_{small}(\tau)$ match or improve upon model-based fitted quantiles (Q_{hat}), despite the nonlinearity of the quantile functions in the model (21).

4.3 Uncertainty Quantification

Next, we assess uncertainty quantification for the posterior action (9) via 95% posterior interval estimates. Specifically, we construct intervals from the posterior draws of (9) for two subsets: the smallest acceptable subset $S_{small}(\tau)$ and the full set of covariates $S_{full} = \{1, \dots, p\}$. By design, $S_{small}(\tau)$ is sparse, so the interval estimates under (9) for any covariates omitted from $S_{small}(\tau)$ are null. Since S_{full} includes all covariates, it circumvents this issue. We compare these interval estimates to the 95% posterior credible intervals from AL_{Bayes} for each τ .

The intervals are evaluated for *calibration*, measured by the empirical coverage, and

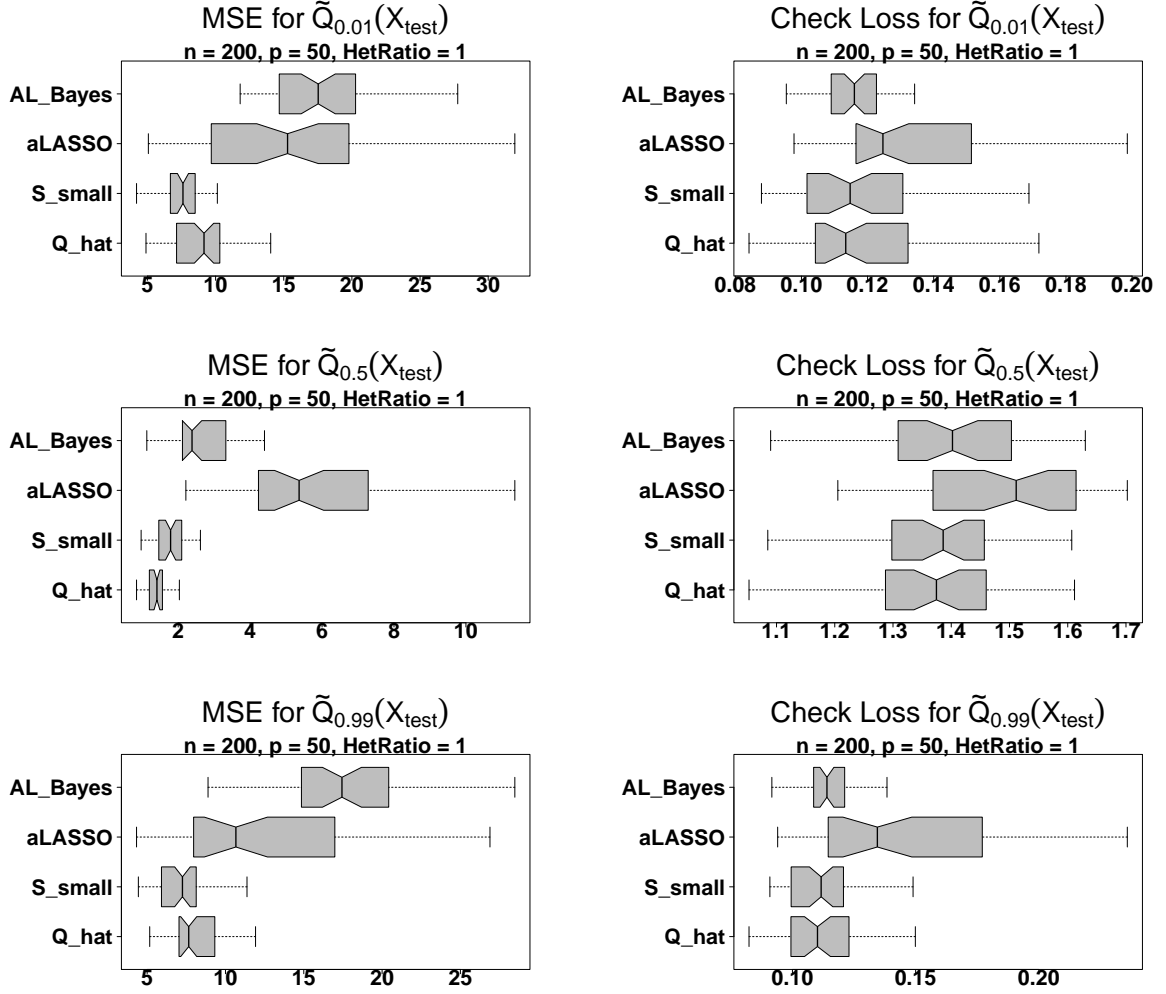


Figure 1: Quantile mean squared error (MSE; left) and check loss (right) among competing quantile regression methods; nonoverlapping notches indicate significant differences between medians, and the dashed vertical line (right) denotes τ . The proposed approach ($S_{\text{small}}(\tau)$) offers substantial improvements in quantile prediction relative to both frequentist and Bayesian competitors, and matches or improves upon the model-based fitted quantiles (Q_{hat}).

sharpness, measured by the average interval widths, in Table 1. Narrow intervals that achieve the 95% nominal coverage are preferred. Most notably, the posterior actions for both S_{full} and $S_{\text{small}}(\tau)$ yield *significantly* more narrow intervals than AL_{Bayes} , often by a factor of 2-5. These effects are especially pronounced for extreme quantiles near zero or one, where AL_{Bayes} is excessively conservative and underpowered. Importantly, both S_{full} and $S_{\text{small}}(\tau)$ maintain the nominal coverage in nearly all settings. As expected, the sparsity of $S_{\text{small}}(\tau)$ produces the most narrow intervals, but also sacrifices empirical coverage for any

active variables excluded from $S_{small}(\tau)$. The results for the other simulation settings are similar, and can be found in the supplementary material (Section E).

$n = 200, p = 50, \text{HetRatio} = 1$								
	τ	0.01	0.05	0.25	0.5	0.75	0.95	0.99
Coverage Rate	$S_{small}(\tau)$	0.83	0.86	0.88	0.90	0.88	0.85	0.83
	S_{full}	0.98	0.97	0.95	0.94	0.95	0.97	0.97
	AL_{Bayes}	0.98	0.97	0.94	0.94	0.95	0.97	0.98
Avg. 95% CI Width	$S_{small}(\tau)$	1.23	1.13	0.94	0.81	0.94	1.17	1.27
	S_{full}	3.56	2.87	2.02	1.76	2.03	2.90	3.60
	AL_{Bayes}	8.64	4.95	3.10	2.73	3.04	4.99	9.19

$n = 500, p = 20, \text{HetRatio} = 1$								
	τ	0.01	0.05	0.25	0.5	0.75	0.95	0.99
Coverage Rate	$S_{small}(\tau)$	0.92	0.91	0.90	0.89	0.89	0.94	0.95
	S_{full}	0.93	0.92	0.91	0.91	0.91	0.96	0.97
	AL_{Bayes}	0.94	0.94	0.93	0.94	0.95	0.99	0.99
Avg. 95% CI Width	$S_{small}(\tau)$	0.63	0.51	0.36	0.31	0.37	0.52	0.65
	S_{full}	1.41	1.14	0.83	0.75	0.84	1.15	1.43
	AL_{Bayes}	4.01	2.40	1.43	1.25	1.41	2.42	4.32

Table 1: Coverage rates and average widths of 95% credible intervals for the posterior action (9) with $S_{small}(\tau)$ or S_{full} as well as AL_{Bayes} . The intervals for $S_{small}(\tau)$ and S_{full} are significantly more narrow than those for AL_{Bayes} , especially for quantiles near zero or one, and typically maintain nominal coverage. $S_{small}(\tau)$ sacrifices some coverage in favor of sparsity, and thus provides the most narrow intervals.

4.4 Selection

We evaluate quantile-specific subset selection by computing true positive rates (TPR) and true negative rates (TNR) for the variables selected by $S_{small}(\tau)$, aLASSO and AL_{Bayes} . Here, \mathcal{M} is not a competitor: it does not specify linear quantiles or any mechanism for quantile-specific variable selection. The results are presented in Table 2.

Across all settings, $S_{small}(\tau)$ provides a superior balance between TPR and TNR. AL_{Bayes} is underpowered and overconservative due to the excessively wide posterior credible intervals that are used for selection (see Table 1). The frequentist competitor aLASSO often produces similar TPRs but lower TNRs compared to $S_{small}(\tau)$, and thus selects too

many variables.

Improvements in TPRs for $S_{small}(\tau)$ over aLASSO are most notable for extreme quantiles, though $S_{small}(\tau)$ appears to offer relatively low power in the larger p settings. Considering this exception more carefully, the coefficients $\beta_{het}^*(.01)$ and $\beta_{het}^*(.99)$ are about four times larger in magnitude than $\beta_{hom}^*(\tau)$, so that $\mathbf{X}_{het}\beta_{het}^*(\tau)$ explains the vast majority of the variability in the quantiles for $\tau \in \{0.01, 0.99\}$. This effect is even more pronounced for the $(n, p) = (100, 100)$ setting, where the heterogeneous coefficient is often five to ten times larger for each quantile. For these quantiles, $S_{small}(\tau)$ always includes the heterogeneous predictor, but leaves out the homogeneous predictors, which are less important for predicting those quantiles. This is consistent with the definition of $S_{small}(\tau)$, which seeks to find the *smallest* subset that nearly matches the model-based quantile estimation from \mathcal{M} , and indeed achieves this latter objective (Figure 1).

$n = 200, p = 50, \text{HetRatio} = 1$								
	τ	0.01	0.05	0.25	0.5	0.75	0.95	0.99
TPR	$S_{small}(\tau)$	0.43	0.54	0.69	0.79	0.63	0.57	0.46
	aLASSO	0.21	0.76	0.89	0.95	0.89	0.71	0.27
	AL_{Bayes}	0.00	0.02	0.22	0.35	0.23	0.03	0.00
TNR	$S_{small}(\tau)$	0.88	0.85	0.82	0.84	0.83	0.85	0.87
	aLASSO	0.88	0.55	0.29	0.27	0.28	0.54	0.83
	AL_{Bayes}	0.97	0.97	0.97	0.96	0.97	0.97	0.93

$n = 500, p = 20, \text{HetRatio} = 1$								
	τ	0.01	0.05	0.25	0.5	0.75	0.95	0.99
TPR	$S_{small}(\tau)$	0.96	0.98	0.95	1.00	0.92	0.99	0.96
	aLASSO	0.65	0.99	0.99	1.00	0.98	0.99	0.72
	AL_{Bayes}	0.00	0.31	0.83	0.99	0.86	0.36	0.00
TNR	$S_{small}(\tau)$	0.94	0.93	0.93	0.91	0.92	0.93	0.94
	aLASSO	0.87	0.71	0.58	0.52	0.55	0.72	0.82
	AL_{Bayes}	1.00	1.00	0.99	0.99	0.99	1.00	1.00

Table 2: True positive rates (TPR) and true negative rates (TNR) for variable selection averaged across simulations. The proposed approach ($S_{small}(\tau)$) neatly balances TPR and TNR. The Bayesian competitor (AL_{Bayes}) is significantly underpowered due to excessively wide posterior credible intervals, while the frequentist competitor (aLASSO) often overselects variables (low TNRs). The results for the $(n, p) = (100, 100)$ are qualitatively similar, but with lower TPR due to the disproportionately large effect of the heterogeneous covariate on the response

5 Social Stressors, Environmental Exposures, and Childhood Educational Outcomes

Childhood educational outcomes are affected by social stressors (e.g., poverty, structural racism, high unemployment) and environmental exposures (e.g., poor air quality, lead exposure), which often cumulate in the same communities (Miranda et al., 2007; Bravo et al., 2024). Thus, there is urgency to quantify and characterize these effects and initiate well-informed policy interventions, especially given the strong links between educational attainment and adult health. However, far less is known about the differential impacts of social stressors and environmental exposures on low-, medium-, and high-achieving students. Such information is critical for understanding the factors that shape educational outcomes and for recommending policy interventions, especially to support at-risk students. Thus, quantile regression is an informative tool—especially with the ability to quantify effect directions and magnitudes, measure and report uncertainty, and provide quantile-specific subset selection.

To analyze these relationships, we construct a large cohort ($n = 23,232$) of North Carolina (NC) students by linking three administrative datasets (CEHI, 2020): **NC Detailed Birth Records**, which provides maternal and infant characteristics for all documented live births in NC; **NC Blood Lead Surveillance**, which includes blood lead level (`Blood_lead`) measurements for each child; and **NC Standardized Testing Data**, which contains standardized (by the year of test, 2010–2012) fourth end-of-grade (EoG) reading scores for each student (`Reading_Score`). Because these datasets also include residential information, we are able to calculate indices of neighborhood deprivation (NDI) and racial residential isolation (RI), which measure students’ exposure to poverty and structural racism, respectively. The full collection of variables is summarized in Table 3.

We augment the covariates in Table 3 with interactions between mother’s race (`mRace`)

Birth information	
mEdu	Mother’s education group at the time of birth (No high school diploma, High school diploma, College diploma)
mRace	Mother’s race/ethnicity group (Non-Hispanic (NH) White, NH Black)
BWTpct	Birthweight percentile
mAge	Mother’s age at the time of birth
Male	Male infant? (1 = Yes)
Smoker	Mother smoked? (1 = Yes)
NotMarried	Not married at time of birth (1 = Yes)
NOPNC	Mother received pre-natal care before birth? (1 = No prenatal care)
Weeks_Gestation	Gestational period (in weeks)
Education/End-of-grade (EoG) test information	
Reading_Score	Standardized score for the (chronologically first) 4th EoG reading test
Blood lead surveillance	
Blood_lead	Blood lead level (micrograms per deciliter)
Social/Economic status	
EconDisadvantage	Participation in Child Nutrition Lunch Program? (1 = Yes)
NDI	Neighborhood Deprivation Index, at time of EoG test
RI	Racial residential isolation, at time of EoG test

Table 3: Variables in the North Carolina dataset. Data are restricted to children with NH Black or NH White mothers (Bravo et al., 2022), 30-42 weeks of gestation, 0-104 weeks of age-within-cohort, mother’s age 15-44, Blood_Lead ≤ 10 , birth order ≤ 4 , no status as an English language learner, and residence in NC at the time of birth and the time of 4th EoG test. Numeric covariates are centered and scaled to mean zero and standard deviation 0.5.

and each of blood lead level (`blood_lead`), neighborhood deprivation (`NDI`), and racial residential isolation (`RI`). Crucially, these interactions allow us to assess whether the (possibly heterogeneous) effects of environmental exposures and social stressors on educational outcomes also differ between race groups.

We fit the Bayesian LL-LS model (21) to this dataset of $n = 23,232$ students with $p = 18$ covariates. Posterior and posterior predictive diagnostics (Gelman et al., 1996) demonstrate that the model is well-calibrated to the data, and notably provide key evidence for heteroscedasticity of $Y \mid \mathbf{x}$ (Section F.2 of the supplement). Thus, we anticipate that quantile regression may detect heterogeneous covariate effects.

Quantile-specific acceptable families $\mathbb{A}_\varepsilon(\tau)$ are constructed for $\tau \in \{0.01, 0.05, 0.25, 0.5, 0.75, 0.95, 0.99\}$ under \mathcal{M} using the subset search and selection techniques from Sections 2-3. Many of the demographic and socioeconomic covariates (Table 3) are strongly correlated (see Section F.1 of the supplement for the correlations between predictors). As a result, there are likely many subsets that perform similarly—which is captured by the acceptable family $\mathbb{A}_\varepsilon(\tau)$, but *not* any single “best” subset. In particular, we identify several hundred acceptable subsets for each τ . We summarize the acceptable family $\mathbb{A}_\varepsilon(\tau)$ using quantile-specific coefficient estimations and intervals for $S_{small}(\tau)$ along with the quantile-specific variable importance (19). For comparison, we include point estimates from aLASSO and posterior means and 95% credible intervals from AL_{Bayes} for the quantile-specific linear coefficients.

In Figure 2 we report the estimates and uncertainty quantification among the competing methods for the main effects that do not include interactions with race. Some of the covariates are not selected by $S_{small}(\tau)$ or aLASSO for certain quantiles, so the resulting point estimates (and intervals for $S_{small}(\tau)$) are fixed at zero. The variables **Weeks_Gestation** and **NOPNC** do not belong to $S_{small}(\tau)$ for any τ , and thus are omitted.

The magnitude and direction of the coefficient estimates from S_{small} reveal numerous interesting patterns. First, the point estimates for **EconDisadv** and **Male** are negative across all quantiles, but the effects on reading scores are more pronounced for *lower* quantiles. This suggests that the discrepancies between male and female students, and between students who are economically disadvantaged and students who are not, are greater for lower-scoring students. Other covariates have little variability over τ ; the coefficients for **BWTpct** and **mAge** are relatively flat, demonstrating that birthweight percentile and mother’s age at the time of birth have significant, yet homogeneous impacts across the distribution of $Y \mid \mathbf{x}$.

The 95% credible intervals for the coefficients in $S_{small}(\tau)$ are substantially more narrow than AL_{Bayes} , which is consistent with the simulation results (Section 4.4). This advantage

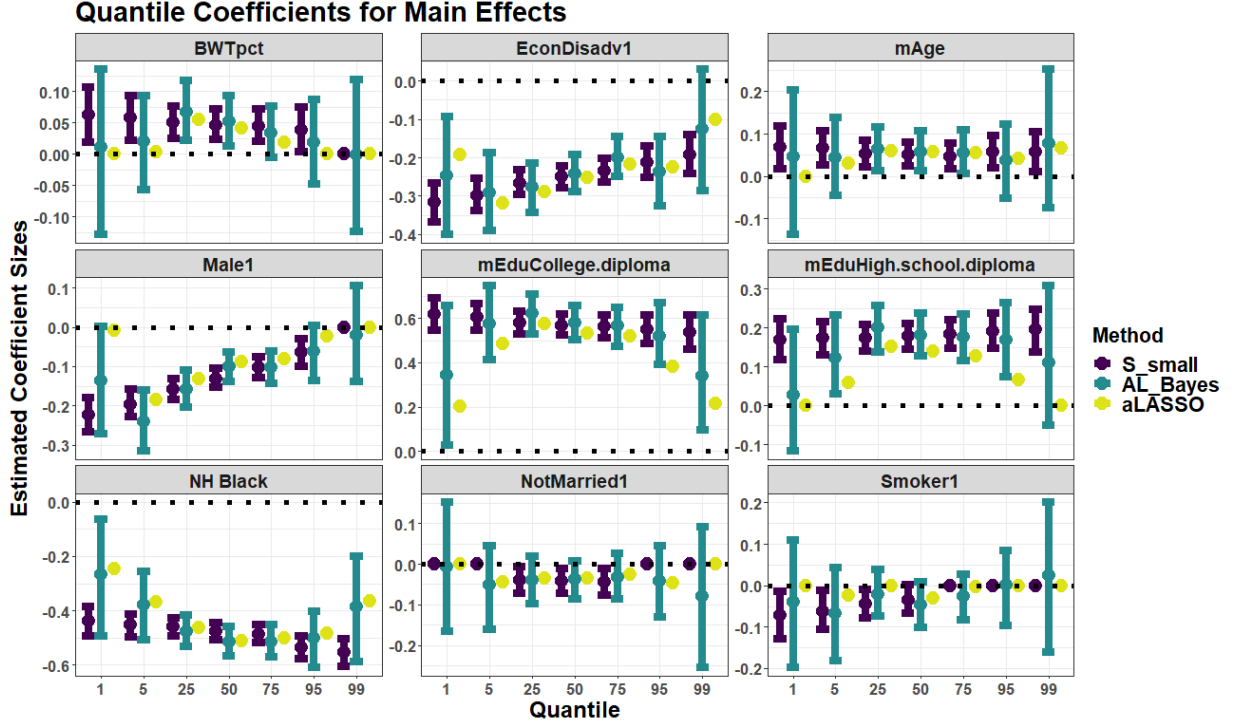


Figure 2: Quantile-specific point estimates and 95% credible intervals for main effects (not interacted with mother’s race) under S_{small} (purple), AL_{Bayes} (green) and $aLASSO$ (yellow); the horizontal line denotes zero. Under the proposed approach (S_{small}), we identify several heterogeneous effects on reading scores, including gender and economically disadvantaged students. Other effects, such birthweight percentile and mother’s age, are relatively homogeneous. By contrast, AL_{Bayes} exhibits excessively wide credible intervals, especially for extreme quantiles, while the $aLASSO$ estimates are highly variable and nonsmooth across τ .

is most pronounced in the extreme quantiles near zero or one, and helps to uncover clear patterns in covariate heterogeneity. The $aLASSO$ estimates vary erratically across τ , often with large jumps for extreme quantiles. This effect is notable for the **Male** coefficients: the estimated coefficients are increasingly negative for smaller τ , yet the estimate at $\tau = 0.01$ is zero. Similar patterns persist for **mEdu**, **EconDisadv** and **mRace**, and undermine the interpretability of the quantile-specific coefficients under $aLASSO$.

The main and race-interaction effects for the social stressors and environmental exposures are presented in Figure 3. Here, the main effects refer specifically to the NH White group, while the interaction effects refer to the differences between these effects for NH Black students and NH White students. First, lead exposure is especially detrimental for lower-scoring students, with no estimated differences between the race groups. Second,

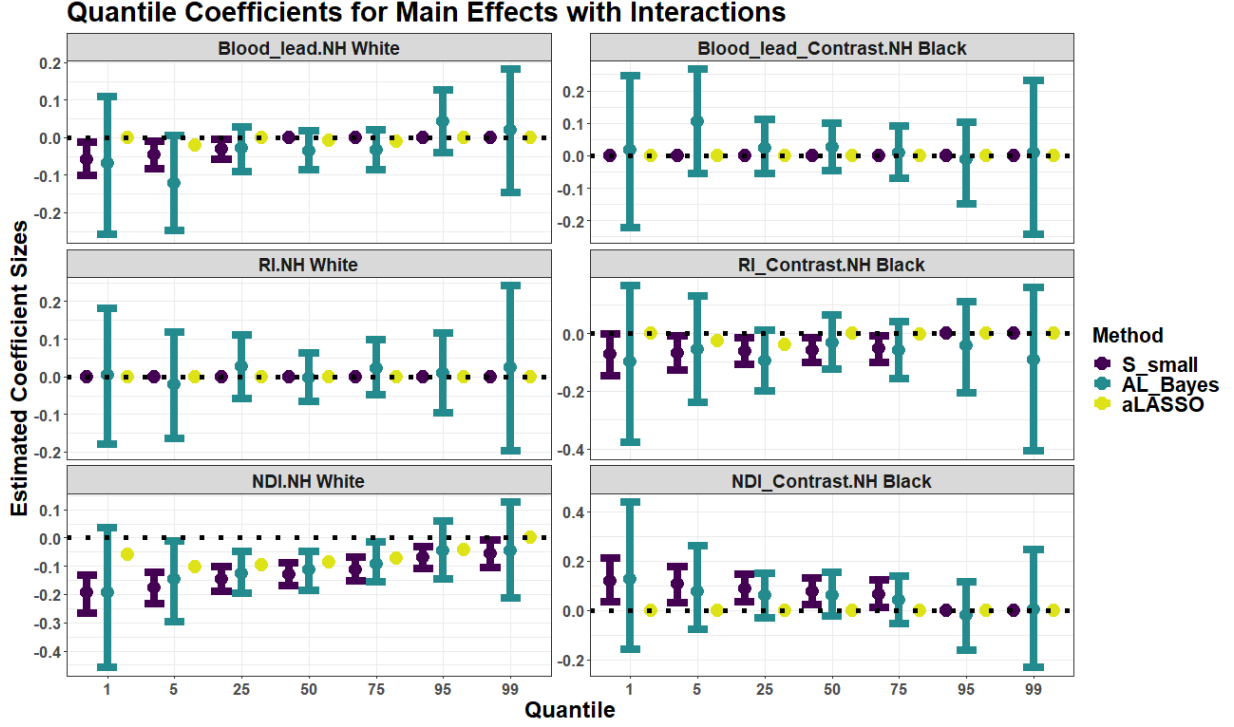


Figure 3: Quantile-specific point estimates and 95% credible intervals for social and environmental exposures that are interacted with mother’s race under S_{small} (purple), AL_{Bayes} (green) and aLASSO (yellow); the horizontal line denotes zero. The main effects (left) refer specifically to the NH White group, while the interaction effects (right) refer to the differences between these effects for NH Black students and NH White students. Under $S_{small}(\tau)$, the `blood_lead` effects are increasingly negative for $\tau < 0.5$, with no clear differences between NH Black and NH White students. RI similarly exhibits an increasingly negative effect for lower quantiles, but only for NH Black students. Finally, the NDI effects are heterogeneous and increasingly negative for lower quantiles among NH White students, but for NH Black students, the effects are negative yet homogeneous across τ . Again, AL_{Bayes} produces excessively wide credible intervals, while aLASSO only identifies nonzero effects for NDI among NH White students.

the estimated RI effect is similarly detrimental for lower-scoring students, but only for NH Black students. Finally, NDI exhibits a heterogeneous effect for NH White students, with increasingly negative effects for lower-scoring students. The positive and heterogeneous effects for the NDI contrast term must be interpreted carefully: in conjunction with the main effect estimates, these estimates indicate that the effect of NDI is still negative for NH Black students, but now homogeneous across τ .

Once again, AL_{Bayes} produces excessively wide credible intervals, which obscures important heterogeneity patterns across τ . Similarly, aLASSO only identifies nonzero effects for NDI among NH White students; yet even these estimated effects fail to satisfy monotonicity

across τ .

Finally, we present the variable importance $VI_j(\tau)$ for each covariate j and quantile τ in Figure 4. $VI_j(\tau)$ seeks to summarize the acceptable family $\mathbb{A}_\varepsilon(\tau)$ of near-optimal subsets by tallying the proportion of acceptable subsets in which each variable belongs. In particular, we identify *keystone covariates* that satisfy $VI_j(\tau) > 0.9$ for any τ , and thus are valuable covariates that belong to at least 90% of acceptable subsets.

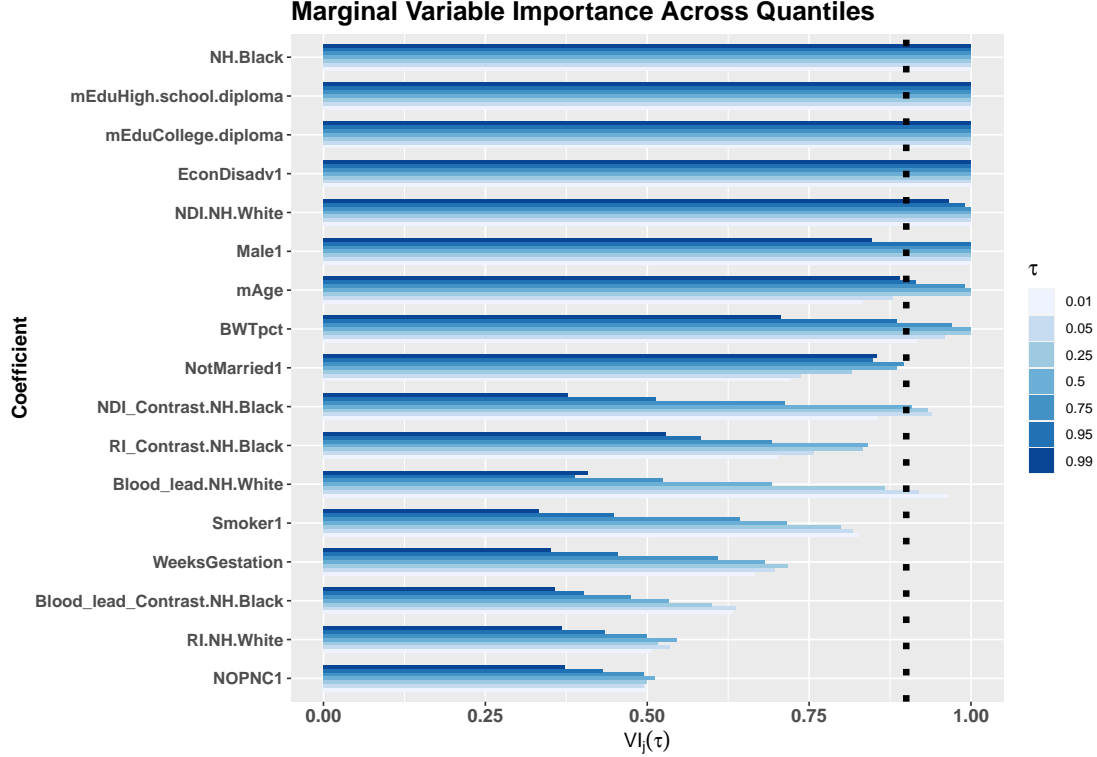


Figure 4: Variable importance $VI_j(\tau)$ from (19), colored by quantile; the dashed line indicates 0.90. Large values indicate that the covariate appears in many of the acceptable subsets. **mEdu**, **mRace** and **EconDisadvantage** appear in all acceptable subsets for all quantiles, while several of the environmental and social factors exhibit heterogeneous variable importance, often with increasing $VI_j(\tau)$ for smaller quantiles (See Section E).

Most notably, **mEdu**, **mRace** and **EconDisadvantage** appear in all acceptable subsets across quantiles. These keystone covariates are essential for near-optimal prediction across the entire distribution of reading scores $Y \mid \mathbf{x}$. Heterogeneous and large $VI_j(\tau)$ effects are apparent for **blood_lead** main effects (i.e., for NH White students) and **NDI** and **RI** contrasts (i.e., differences between NH Black and NH White students), with increasing variable

importance for lower quantiles. Similarly heterogeneous and large variable importance are observed for `mAge`, `BWTpct`, and `NotMarried`.

In aggregate, our analysis uncovers substantial heterogeneity in the effects of environmental exposures, social stressors, and other key factors on reading scores. Notably, both the coefficient (point and interval) estimates (Figures 2-3) and the variable importance (Figure 4) highlight numerous increasingly adverse effects for lower-scoring students. These effects include lead exposure, economic disadvantage, racial residential isolation, and neighborhood deprivation, among others, with some differential effects by race. We also note that this discovery was consistent when applying the subset search and selection techniques to the AL_{Bayes} model, see Section F.3 of the supplement for complete results. These new findings contribute to our understanding of the disparities in childhood development and educational outcomes.

6 Conclusion

We proposed a novel approach to Bayesian linear quantile regression with subset selection. The procedure features two stages, but operates within a single, coherent, Bayesian modeling and decision analysis framework. First, the analyst curates a Bayesian regression model to best represent the conditional distribution $Y \mid \mathbf{x}$. Then, based on the conditional quantiles from the Bayesian model, we apply a decision analysis to extract linear and quantile-specific coefficient estimates, uncertainty quantification, and subset selection. This approach uses a quantile-focused squared error loss function, which maintains a close, theoretical connection to density regression on the Wasserstein geometry. Crucially, this loss function enables closed-form computation of optimal linear coefficients and uncertainty quantification for any subset of predictors. We leverage these computational results to unlock state-of-the-art subset search and selection algorithms that were previously available only for mean regression. Our strategy prioritizes accumulation of many, highly predictive

subsets to form a quantile-specific acceptable family, which we summarize by reporting the smallest acceptable subset (in accordance with the parsimony principle) and measures of variable importance.

There are several advantages of the proposed approach relative to existing frequentist and Bayesian quantile regression methods. First, the framework is valid under *any* Bayesian regression model. Thus, the analyst can prioritize calibrated modeling of the observed data without the need to accommodate quantile-specific modeling requirements, such as inadequate likelihoods or unwieldy constraints. Second, the decision analysis conveys regularization, uncertainty quantification, and smoothness across quantiles from the underlying Bayesian regression model. This occurs despite the fact that the decision analysis is applied separately for each quantile, yielding straightforward and efficient implementations. Finally, our approach delivers subset search and selection for quantile regression, which has remained elusive among frequentist and Bayesian methods.

These benefits translate to significant empirical improvements. In an extensive simulation study, we found that the proposed approach produces more accurate quantile predictions, more precise (yet calibrated) uncertainty quantification, and more powerful variable selection for quantile regression coefficients.

We applied our methods to analyze the effects of social stressors, environmental exposures, and other key factors on 4th end-of-grade reading test scores for a large cohort of children in North Carolina. Our analysis revealed several important and unique insights into educational inequities. Most notably, we found that lead exposure, economic disadvantage, racial residential isolation, and neighborhood deprivation more adversely impact reading test scores for lower-scoring students. These effects exhibited heterogeneity not only across quantiles, but also across race groups. Furthermore, we found that these covariates tended to be more important for prediction of the lower quantiles of educational outcomes. These alarming results have important implications for childhood development

and educational attainment, and may inform policy to develop and target intervention strategies.

With such encouraging results, there are numerous promising directions for future research. Although we have focused on linear quantile regression, our decision analysis framework can be readily extended to nonlinear quantile-specific summaries, such as trees or additive models. This enhanced flexibility may be useful for quantile estimation under nonlinear Bayesian models, such as heteroscedastic Bayesian additive regression trees (Pratola et al., 2020). Further, our approach is not limited to Bayesian models with Gaussian errors. A useful extension would be to consider Bayesian models for extreme events (Fagnant et al., 2020), with a customized decision analysis for estimation, uncertainty quantification, and selection. Finally, the proposed (linear) quantile predictions are quick to compute with minimal storage requirements, and thus may be used to provide fast, model-based prediction intervals, especially when the underlying Bayesian model does not admit efficient posterior predictive sampling.

7 Acknowledgments

The findings and conclusions in this presentation or publication are those of the authors and do not necessarily represent the views of the North Carolina Department of Health and Human Services, Division of Public Health, the National Institutes of Health, the Army Research Office, or the U.S. Government. The U.S. Government is authorized to reproduce and distribute reprints for Government purposes notwithstanding any copyright notation herein.

Research reported in this publication was supported by the National Institute of Environmental Health Sciences of the National Institutes of Health under award number R01ES028819, National Science Foundation under award number SES-2214726, and the Army Research Office under award number W911NF-20-1-0184.

References

- Alhamzawi, R. and Ali, H. T. M. (2020), “Brq: An R package for Bayesian quantile regression,” *Metron*, 78, 313–328.
- Alhamzawi, R., Yu, K., and Benoit, D. F. (2012), “Bayesian adaptive Lasso quantile regression,” *Statistical Modelling*, 12, 279–297.
- Bassett, G. W. and Chen, H.-L. (2002), “Portfolio style: Return-based attribution using quantile regression,” *Economic applications of quantile regression*, 293–305.
- Belloni, A. and Chernozhukov, V. (2011), “L1-penalized quantile regression in high-dimensional sparse models,” *The Annals of Statistics*, 39, 82 – 130, URL <https://doi.org/10.1214/10-AOS827>.
- Benoit, D. F. and Van den Poel, D. (2017), “bayesQR: A Bayesian approach to quantile regression,” *Journal of Statistical Software*, 76, 1–32.
- Bertsimas, D., King, A., and Mazumder, R. (2016), “Best subset selection via a modern optimization lens,” *The Annals of Statistics*, 44, 813 – 852, URL <https://doi.org/10.1214/15-AOS1388>.
- Bondell, H. D., Reich, B. J., and Wang, H. (2010), “Noncrossing quantile regression curve estimation,” *Biometrika*, 97, 825–838.
- Bravo, M. A., Kowal, D. R., Zephyr, D., Feldman, J., Ensor, K., and Miranda, M. L. (2024), “Spatial Variability in Relationships between Early Childhood Lead Exposure and Standardized Test Scores in Fourth Grade North Carolina Public School Students (2013–2016),” *Environmental Health Perspectives*, 132, 097003.
- Bravo, M. A., Zephyr, D., Kowal, D., Ensor, K., and Miranda, M. L. (2022), “Racial residential segregation shapes the relationship between early childhood lead exposure and

- fourth-grade standardized test scores,” *Proceedings of the National Academy of Sciences*, 119, e2117868119.
- Carpenter, B., Gelman, A., Hoffman, M. D., Lee, D., Goodrich, B., Betancourt, M., Brubaker, M. A., Guo, J., Li, P., and Riddell, A. (2017), “Stan: A probabilistic programming language,” *Journal of statistical software*, 76.
- CEHI (2020), URL https://www.cehidatahub.org/hub/Cohort_2000. Linked Births, Lead Surveillance, grade 4 End-Of-Grade (EoG) Scores [Data Set].
- Chen, C. W., Dunson, D. B., Reed, C., and Yu, K. (2013), “Bayesian variable selection in quantile regression,” *Statistics and its Interface*, 6, 261–274.
- Dao, M., Wang, M., Ghosh, S., and Ye, K. (2022), “Bayesian variable selection and estimation in quantile regression using a quantile-specific prior,” *Computational Statistics*, 37, 1339–1368.
- Dunson, D. B. and Taylor, J. A. (2005), “Approximate Bayesian inference for quantiles,” *Journal of Nonparametric Statistics*, 17, 385–400.
- Fagnant, C., Gori, A., Sebastian, A., Bedient, P. B., and Ensor, K. B. (2020), “Characterizing spatiotemporal trends in extreme precipitation in Southeast Texas,” *Natural Hazards*, 104, 1597–1621.
- Fasiolo, M., Wood, S. N., Zaffran, M., Nedellec, R., and Goude, Y. (2021), “Fast calibrated additive quantile regression,” *Journal of the American Statistical Association*, 116, 1402–1412.
- Fréchet, M. (1948), “Les éléments aléatoires de nature quelconque dans un espace distancié,” in *Annales de l’institut Henri Poincaré*, volume 10.
- Furnival, G. M. and Wilson, R. W. (2000), “Regressions by leaps and bounds,” *Technometrics*, 42, 69–79.

- Gelman, A., Meng, X.-L., and Stern, H. (1996), “Posterior predictive assessment of model fitness via realized discrepancies,” *Statistica sinica*, 733–760.
- Hahn, P. R. and Carvalho, C. M. (2015), “Decoupling Shrinkage and Selection in Bayesian Linear Models: A Posterior Summary Perspective,” *Journal of the American Statistical Association*, 110, 435–448, URL <https://doi.org/10.1080/01621459.2014.993077>.
- Hofmann, M., Gatu, C., and Kontoghiorghes, E. J. (2007), “Efficient algorithms for computing the best subset regression models for large-scale problems,” *Computational Statistics & Data Analysis*, 52, 16–29.
- Kadane, J. B. and Tokdar, S. T. (2012), “Simultaneous linear quantile regression: A semiparametric Bayesian approach,” *Bayesian Analysis*, 7, 51 – 72, URL <https://doi.org/10.1214/12-BA702>.
- Keil, A. P., Buckley, J. P., O’Brien, K. M., Ferguson, K. K., Zhao, S., and White, A. J. (2020), “A quantile-based g-computation approach to addressing the effects of exposure mixtures,” *Environmental health perspectives*, 128, 047004.
- Koenker, R. and Bassett Jr, G. (1978), “Regression quantiles,” *Econometrica: journal of the Econometric Society*, 33–50.
- Koenker, R., Chernozhukov, V., He, X., and Peng, L. (2017), “Handbook of quantile regression,” .
- Kottas, A. and Gelfand, A. E. (2001), “Bayesian semiparametric median regression modeling,” *Journal of the American Statistical Association*, 96, 1458–1468.
- Kottas, A. and Krnjajić, M. (2009), “Bayesian semiparametric modelling in quantile regression,” *Scandinavian Journal of Statistics*, 36, 297–319.
- Kowal, D. R. (2021), “Fast, Optimal, and Targeted Predictions using Parametrized Decision Analysis,” *Journal of the American Statistical Association*, 1–28.

- (2022), “Bayesian subset selection and variable importance for interpretable prediction and classification,” *Journal of Machine Learning Research*, 23, 1–38, URL <http://jmlr.org/papers/v23/21-0403.html>.
- Kowal, D. R. and Wu, B. (2024), “Monte Carlo inference for semiparametric Bayesian regression,” *Journal of the American Statistical Association*, 1–25.
- Kozumi, H. and Kobayashi, G. (2011), “Gibbs sampling methods for Bayesian quantile regression,” *Journal of statistical computation and simulation*, 81, 1565–1578.
- Lee, E. R., Noh, H., and Park, B. U. (2014), “Model selection via Bayesian information criterion for quantile regression models,” *Journal of the American Statistical Association*, 109, 216–229.
- Li, Y. and Zhu, J. (2008), “L1-norm quantile regression,” *Journal of Computational and Graphical Statistics*, 17, 163–185.
- Miranda, M. L., Kim, D., Galeano, M. A. O., Paul, C. J., Hull, A. P., and Morgan, S. P. (2007), “The relationship between early childhood blood lead levels and performance on end-of-grade tests,” *Environmental health perspectives*, 115, 1242–1247.
- Pandey, G. R. and Nguyen, V.-T.-V. (1999), “A comparative study of regression based methods in regional flood frequency analysis,” *Journal of Hydrology*, 225, 92–101.
- Petersen, A., Liu, X., and Divani, A. A. (2021), “Wasserstein F -tests and confidence bands for the Fréchet regression of density response curves,” *The Annals of statistics*, 49, 590–.
- Pratola, M., Chipman, H., George, E. I., and McCulloch, R. (2020), “Heteroscedastic BART via multiplicative regression trees,” *Journal of Computational and Graphical Statistics*, 29, 405–417.
- Raftery, A. E., Madigan, D., and Hoeting, J. A. (1997), “Bayesian model averaging for linear regression models,” *Journal of the American Statistical Association*, 92, 179–191.

- Reich, B. J., Bondell, H. D., and Wang, H. J. (2009), “Flexible Bayesian quantile regression for independent and clustered data,” *Biostatistics*, 11, 337–352, URL <https://doi.org/10.1093/biostatistics/kxp049>.
- Reich, B. J. and Smith, L. B. (2013), “Bayesian quantile regression for censored data,” *Biometrics*, 69, 651–660.
- Sherwood, B. and Maidman, A. (2017), “rqPen: Penalized quantile regression,” *R package version*, 2.
- Sriram, K., Ramamoorthi, R., and Ghosh, P. (2013), “Posterior consistency of Bayesian quantile regression based on the misspecified asymmetric Laplace density,” *Bayesian Analysis*, 8, 479 – 504, URL <https://doi.org/10.1214/13-BA817>.
- Taddy, M. A. and Kottas, A. (2010), “A Bayesian nonparametric approach to inference for quantile regression,” *Journal of Business & Economic Statistics*, 28, 357–369.
- Wang, L., Wu, Y., and Li, R. (2012), “Quantile regression for analyzing heterogeneity in ultra-high dimension,” *Journal of the American Statistical Association*, 107, 214–222.
- Woody, S., Carvalho, C. M., and Murray, J. S. (2021), “Model Interpretation Through Lower-Dimensional Posterior Summarization,” *Journal of Computational and Graphical Statistics*, 30, 144–161, URL <https://doi.org/10.1080/10618600.2020.1796684>.
- Wu, Y. and Liu, Y. (2009), “Variable selection in quantile regression,” *Statistica Sinica*, 801–817.
- Yang, Y. and He, X. (2012), “Bayesian empirical likelihood for quantile regression,” *The Annals of Statistics*, 40, 1102 – 1131, URL <https://doi.org/10.1214/12-AOS1005>.
- Yao, Y., Vehtari, A., Simpson, D., and Gelman, A. (2018), “Using stacking to average Bayesian predictive distributions (with discussion),” *Bayesian Analysis*, 13, 917 – 1007, URL <https://doi.org/10.1214/17-BA1091>.

Yu, K. and Moyeed, R. A. (2001), “Bayesian quantile regression,” *Statistics & Probability Letters*, 54, 437–447.

Supplement to

“Bayesian Quantile Regression with Subset Selection: A Decision Analysis Perspective”

A Proofs

We present proofs for the main theoretical results presented in the main paper.

Lemma 1. *Suppose $E_{\theta|\mathbf{y}}\|Q_\tau(Y_i | \mathbf{x}_i, \boldsymbol{\theta})\|_2^2 < \infty$ for $i = 1, \dots, n$. For any quantile $\tau \in (0, 1)$ and any subset of predictors $S \subseteq \{1, \dots, p\}$, the optimal action (6) under the quantile-focused squared error loss (7) is*

$$\hat{\boldsymbol{\delta}}_S(\tau) = (\mathbf{X}_S^\top \mathbf{X}_S)^{-1} \mathbf{X}_S^\top \hat{\mathbf{Q}}_\tau(\mathbf{X}) \quad (\text{A.1})$$

with zeros for indices $j \notin S$, where $\hat{Q}_\tau(\mathbf{x}_i) = E_{\theta|\mathbf{y}}\{Q_\tau(Y_i | \mathbf{x}_i, \boldsymbol{\theta})\}$, $\hat{\mathbf{Q}}_\tau(\mathbf{X}) = \{\hat{Q}_\tau(\mathbf{x}_1), \dots, \hat{Q}_\tau(\mathbf{x}_n)\}^\top$, and \mathbf{X}_S the $n \times |S|$ matrix of active covariates for subset S .

Proof. It suffices to observe that $E_{\theta|\mathbf{y}}\|Q_\tau(Y_i | \mathbf{x}_i, \boldsymbol{\theta}) - \mathbf{x}_i^\top \boldsymbol{\delta}_S(\tau)\|_2^2 = E_{\theta|\mathbf{y}}\|\{Q_\tau(Y_i | \mathbf{x}_i, \boldsymbol{\theta}) - \hat{Q}_\tau(\mathbf{x}_i)\} + \{\hat{Q}_\tau(\mathbf{x}_i) - \mathbf{x}_i^\top \boldsymbol{\delta}_S(\tau)\}\|_2^2 = E_{\theta|\mathbf{y}}\|Q_\tau(Y_i | \mathbf{x}_i, \boldsymbol{\theta}) - \hat{Q}_\tau(\mathbf{x}_i)\|_2^2 + E_{\theta|\mathbf{y}}\|\hat{Q}_\tau(\mathbf{x}_i) - \mathbf{x}_i^\top \boldsymbol{\delta}_S(\tau)\|_2^2$ where the first term is finite and does not depend on $\boldsymbol{\delta}_S(\tau)$. The remaining steps constitute an ordinary least squares solution. \square

Corollary 1. *For the location-scale model (4) with linearity $f(\mathbf{x}_i) = \mathbf{x}_i^\top \boldsymbol{\beta}(\tau)$, homoscedasticity $s(\mathbf{x}_i) = \sigma$, and an intercept $x_{i1} = 1$, the optimal action (6) under (7) for the full set*

of covariates is $\hat{\boldsymbol{\delta}}_{\{1,\dots,p\}}(\tau) = [\hat{\beta}_1(\tau), \{\hat{\beta}_j\}_{j=2}^p]$ for any τ , where $\hat{\beta}_1(\tau) = E_{\boldsymbol{\theta}|\mathbf{y}}[\beta_1 + \sigma F^{-1}(\tau)]$ and $\hat{\beta}_j = E_{\boldsymbol{\theta}|\mathbf{y}}\beta_j$ for $j = 2, \dots, p$.

Proof. With $\hat{s}(\mathbf{x}_i) = E_{\boldsymbol{\theta}|\mathbf{y}}\sigma$ for any \mathbf{x}_i , it suffices to observe that under (4), $\hat{Q}_\tau(\mathbf{x}_i) = \hat{\beta}_1(\tau) + \sum_{j=2}^p x_{ij}\hat{\beta}_j$. In addition, for the action using the full set of covariates, the covariate matrix is \mathbf{X} . Plugging this into (8) yields the result. \square

Corollary 2. *For any Bayesian model with linear quantiles $Q_\tau(Y_i | \mathbf{x}_i, \boldsymbol{\theta}) = \mathbf{x}_i^\top \boldsymbol{\beta}(\tau)$, the optimal action (6) under (7) for the full set of covariates is $\hat{\boldsymbol{\delta}}_{\{1,\dots,p\}}(\tau) = \hat{\boldsymbol{\beta}}(\tau)$, where $\hat{\boldsymbol{\beta}}(\tau) = E_{\boldsymbol{\theta}|\mathbf{y}}\boldsymbol{\beta}(\tau)$.*

Proof. The result is immediate using the argument in Corollary 1 and observing that $\hat{\mathbf{Q}}_\tau(\mathbf{X}) = \mathbf{X}\hat{\boldsymbol{\beta}}(\tau)$. \square

Corollary 3. *For the location-scale model (4) with linearity $f(\mathbf{x}_i) = \mathbf{x}_i^\top \boldsymbol{\beta}(\tau)$, homoscedasticity $s(\mathbf{x}_i) = \sigma$, and an intercept $x_{i1} = 1$, the posterior action (9) for the full set of covariates $S = \{1, \dots, p\}$ satisfies*

$$\boldsymbol{\delta}_{\{1,\dots,p\}}(\boldsymbol{\theta}; \tau) \sim p(\boldsymbol{\theta}^* | \mathbf{y})$$

where $\boldsymbol{\theta}^* = [\beta_1 + \sigma F^{-1}(\tau), \{\beta_j\}_{j=2}^p]$.

Proof. For the homoscedastic linear regression, $Q_\tau(\mathbf{Y} | \mathbf{X}, \boldsymbol{\theta}) = [\{\beta_1 + \sigma F^{-1}(\tau)\} + \sum_{j=2}^p x_{ij}\beta_j]_{i=1}^n$. Therefore, for the full set of covariates and any quantile, (9) is equal in distribution to the regression coefficients under the model \mathcal{M} posterior, with only the intercept term varying as a function of the quantile. \square

Lemma 2. *Let $\boldsymbol{\delta}(\mathbf{x}; \tau) = \mathbf{x}^\top \boldsymbol{\delta}_S(\tau)$ for any \mathbf{x} and any subset S of covariates. Then the minimizer of (13), without a density restriction, is given by the quantile estimators $\hat{\boldsymbol{\delta}}(\mathbf{x}; \tau_m) = \mathbf{x}^\top \hat{\boldsymbol{\delta}}_S(\tau_m)$ with $\hat{\boldsymbol{\delta}}_S(\tau_m)$ computed from (8) separately for each $m = 1, \dots, \ell$.*

Proof. It suffices to observe that objective in (13) may be expanded as $\sum_{\tau=\tau_1}^{\tau_\ell} E_{\boldsymbol{\theta}|\mathbf{y}} \sum_{i=1}^n \|Q_\tau(Y_i | \mathbf{x}_i, \boldsymbol{\theta}) - \mathbf{x}_i^\top \boldsymbol{\delta}_S(\tau)\|_2^2$, and since the optimization is unconstrained for $\boldsymbol{\delta}_S(\tau)$ across τ , the sum-

mands may be optimized separately. Applying Lemma 2.1 separately for each τ_m yields the result.

□

B Detailed Algorithm 1

We present specific computations required for each step in Algorithm 1:

C Hierarchical Specification of the LL-LS Model

We specify the following priors for estimation of the LL-LS model (21) for the simulation study and real data analysis in Sections 4-5.

$$y_i \sim \text{Normal}(\mathbf{x}_i^\top \boldsymbol{\xi}, \{\boldsymbol{\sigma} \exp(\mathbf{x}_i^\top \boldsymbol{\gamma})\}^2) \quad (\text{C.1})$$

$$\xi_j \stackrel{\text{indep}}{\sim} \text{Normal}(0, \lambda_{\xi_j}), j \in \{2, \dots, p\}, \quad \gamma_j \stackrel{\text{indep}}{\sim} \text{Normal}(0, \lambda_{\gamma_j}), j \in \{2, \dots, p\} \quad (\text{C.2})$$

$$\lambda_{\gamma_j}, \lambda_{\xi_j} \sim \text{Cauchy}^+(0, 5), j \in \{2, \dots, p\} \quad (\text{C.3})$$

$$\sigma^2 \sim \text{Inverse-Gamma}(1/2, 1/2) \quad (\text{C.4})$$

Here, Cauchy^+ is the half cauchy distribution. In addition, we specify flat priors for the intercept terms, i.e. $\beta_1, \gamma_1 \propto 1$. The model is estimated in the **STAN** programming language in R.

D Prescreening for the BBA Algorithm

For the simulation setting involving $p = 50$ covariates in Section 4, we adopt a prescreening strategy for the LL-LS model \mathcal{M} to narrow the class of candidate subsets. In general, the BBA algorithm is efficient for $p \leq 35$, and acceptable subsets are more interpretable with

greater levels of sparsity.

The prescreening strategy proceeds as follows: We first compute the posterior mean for each ξ_j and γ_j , denoted $\hat{\xi}_j$ and $\hat{\gamma}_j$, respectively. Then, we identify the top 35 covariates for which $|\hat{\gamma}_j| + |\hat{\xi}_j|$ is greatest. These covariates, and the ensuing submatrix is passed into the BBA algorithm to provide candidate subsets for curation of the acceptable family, as described in Section 3.2.

E Further Simulation Results

For the $(n, p) = (100, 100)$ setting, we utilized the `Brq` package in `R` under default settings for the adaptive LASSO prior (Alhamzawi and Ali, 2020). Default settings for the adaptive LASSO quantile regressions in `BayesQR` repeatedly caused our local machine to crash whenever $p \geq n$. Upon correspondence with the authors of `BayesQR`, the code malfunction could be attributed to regression coefficient initialization at OLS estimates, which are not identified in $p \geq n$ regimes. Fortunately, the MCMC algorithms are quite similar between software packages and the results were minimally affected and consistent with what is presented in the paper.

E.1 Uncertainty Quantification

We complete the information presented in Table 2 with the nominal coverage rates and interval widths in the other simulation settings in Table 4. The results are consistent with what is presented in the main paper - S_{small} and S_{full} are significantly more sharp and calibrated than the Bayesian and frequentist alternatives.

E.2 Selection with Independent Covariates

We compute average TPRs and TNRs for each $(n, p, \text{HetRatio})$ setting where the covariates x_{ij} are simulated independently from a $\text{uniform}(0, 1)$ in Table 5. Once again, the proposed

approach balances TPR and TNR well, with the frequentist competitor once again overly dense (low TNRs), and AL_{Bayes} underpowered (low TPRs).

E.3 Predictive Evaluations

We complete the results presented in Figure 1 for the remaining simulation settings, metrics and quantiles in Figures E.3- E.16. The results are consistent with what is presented in the paper: $S_{small}(\tau)$ demonstrates better predictive capabilities and is more calibrated than the frequentist and Bayesian competitors, with pronounced improvement at extreme quantiles. We note that the results presented here and in the main paper are qualitatively similar to simulations carried out under the same generating model for the response and $(n, p, \text{HetRatio})$ settings, but with independent covariates.

Figure E.1: MSE: $n = 500, p = 20, \text{HetRatio} = 0.5$

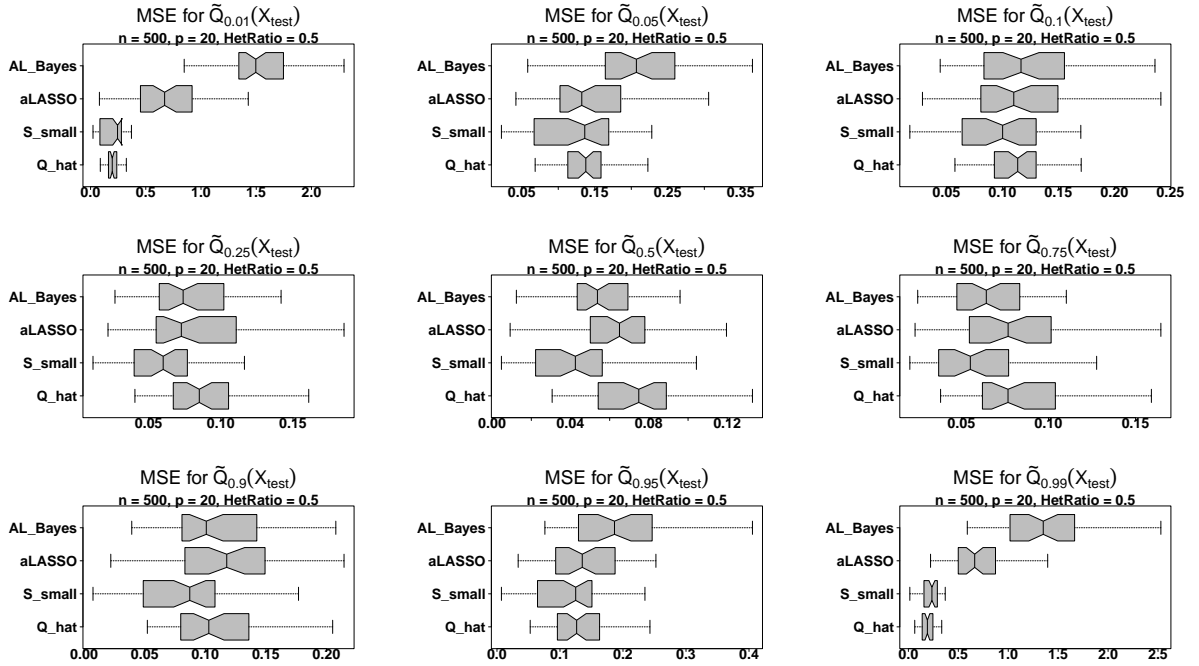


Figure E.2: MSE: $n = 500, p = 20, \text{HetRatio} = 1$

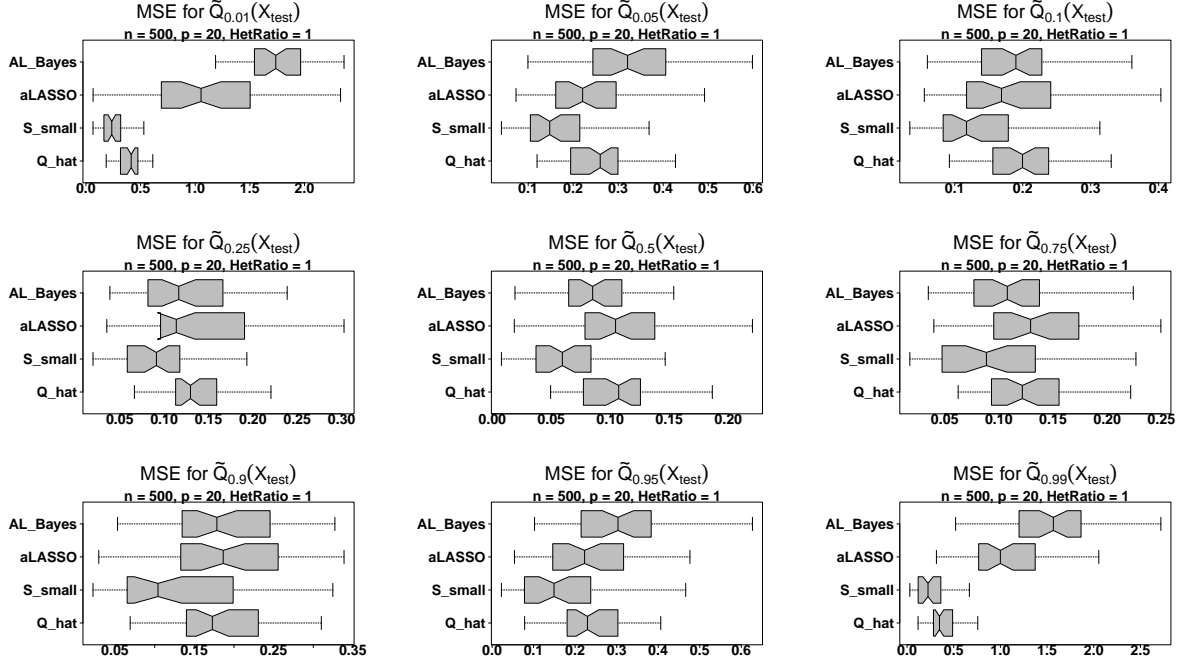


Figure E.3: MSE: $n = 100, p = 100, \text{HetRatio} = 0.5$

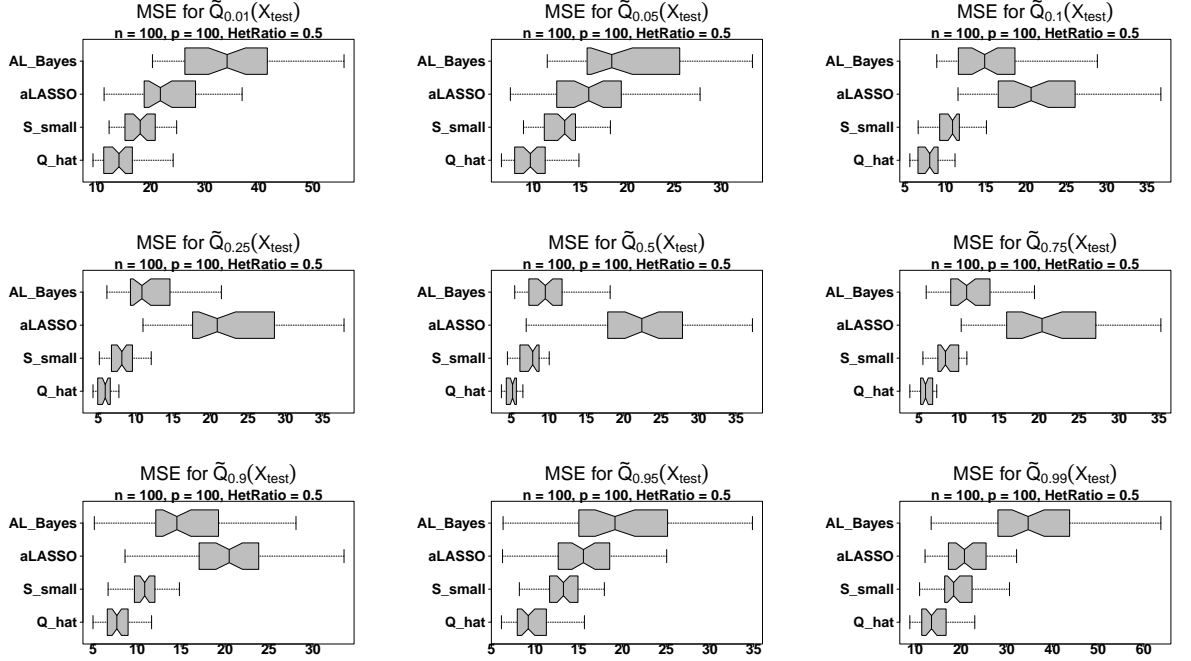


Figure E.4: MSE: $n = 100, p = 100, \text{HetRatio} = 1$

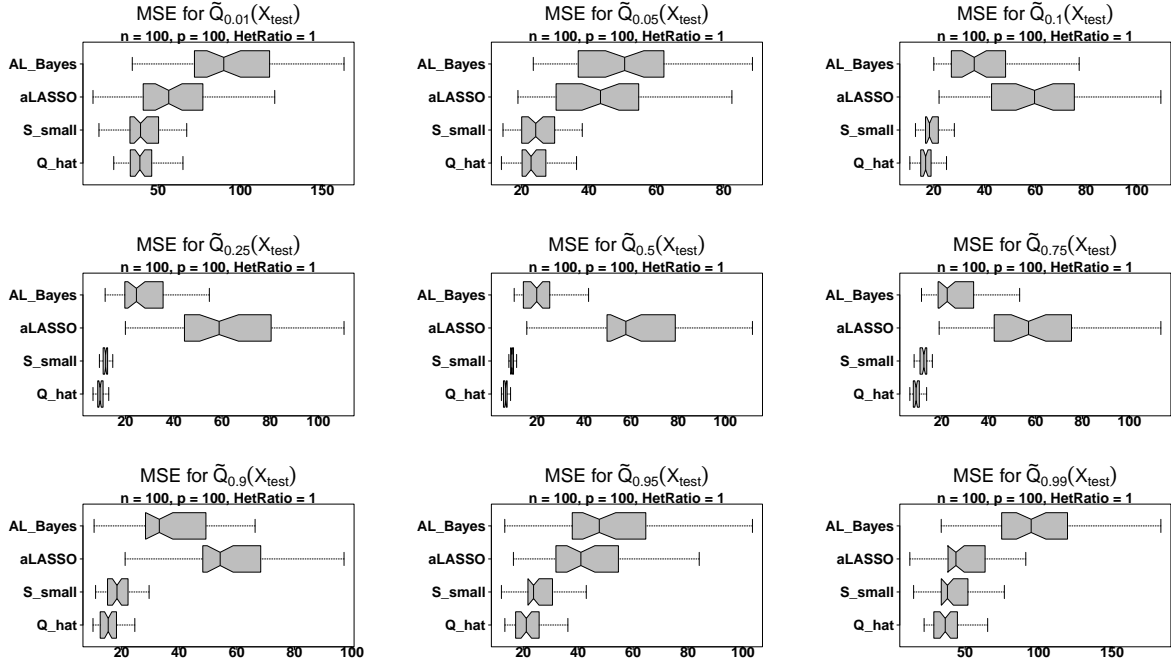


Figure E.5: MSE: $n = 200, p = 50, \text{HetRatio} = 0.5$

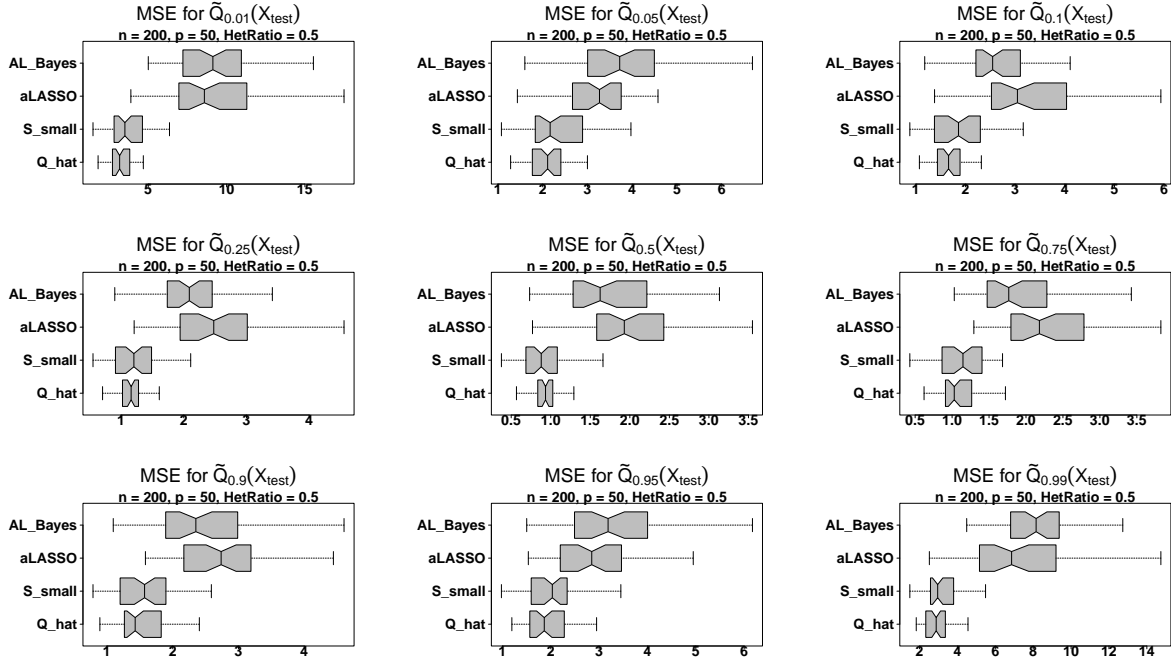


Figure E.6: MSE: $n = 200, p = 50, \text{HetRatio} = 1$

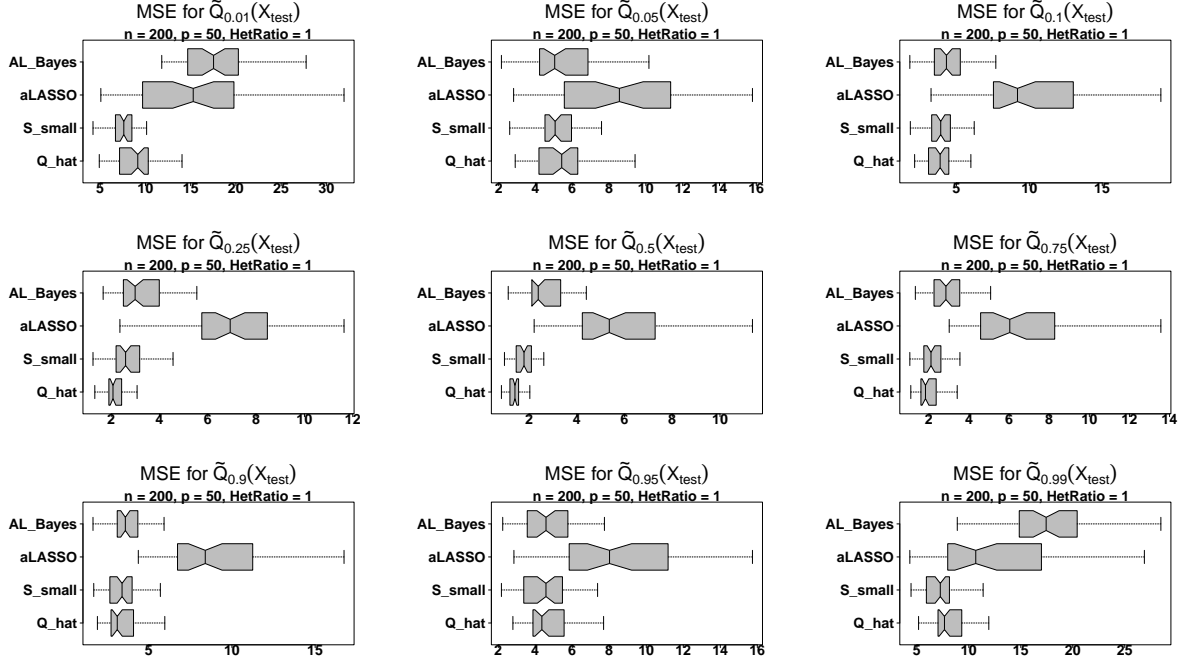


Figure E.7: Check Loss: $n = 500, p = 20, \text{HetRatio} = 0.5$

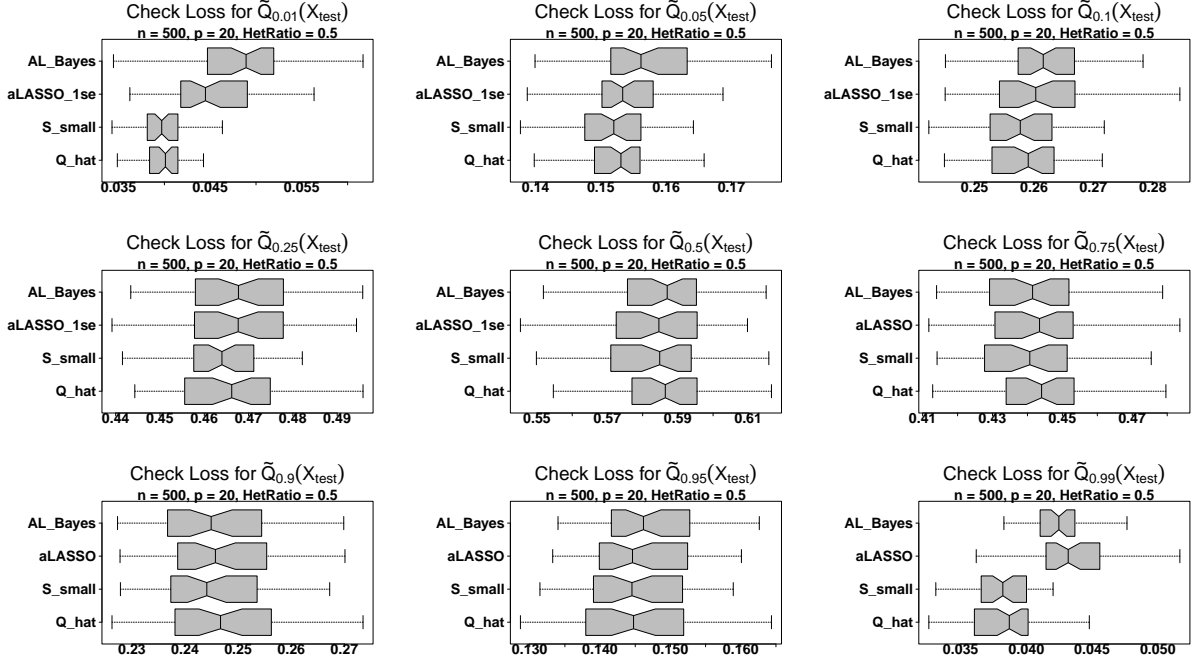


Figure E.8: Check Loss: $n = 500, p = 20, \text{HetRatio} = 1$

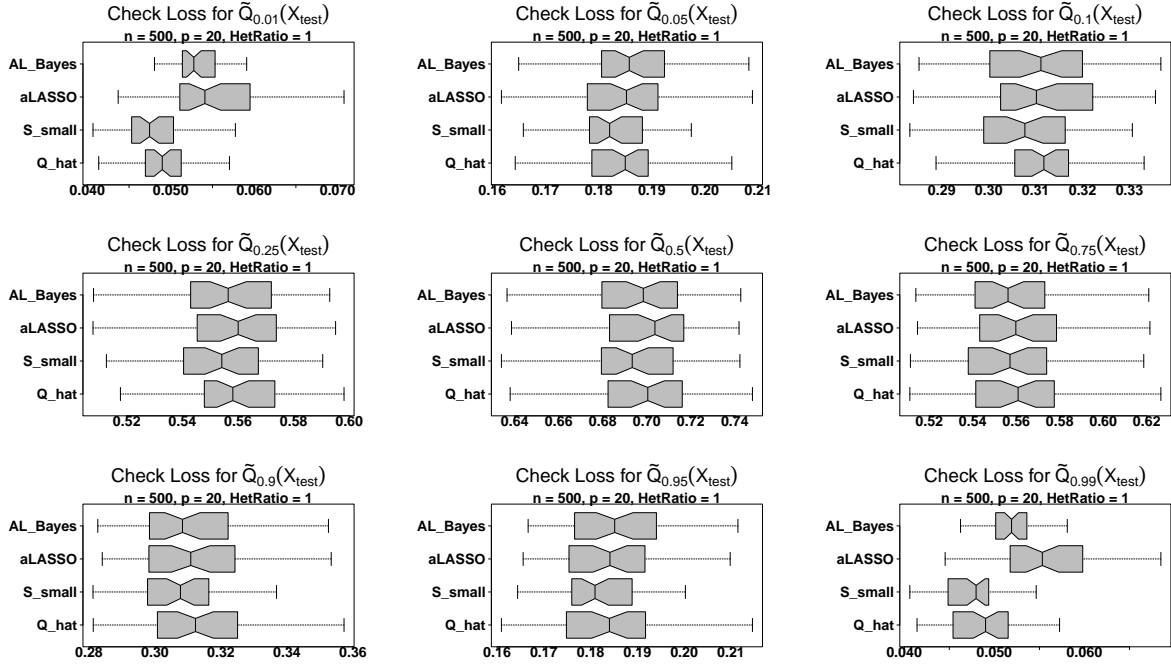


Figure E.9: Check Loss: $n = 100, p = 100, \text{HetRatio} = 0.5$

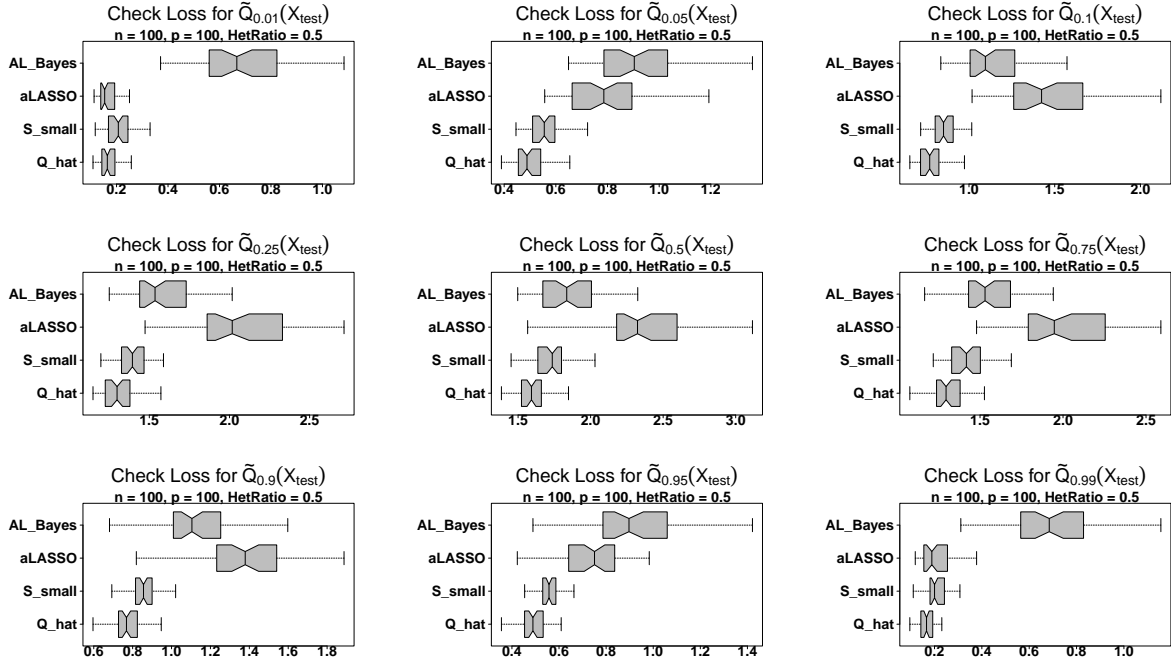


Figure E.10: Check Loss: $n = 100, p = 100, \text{HetRatio} = 1$

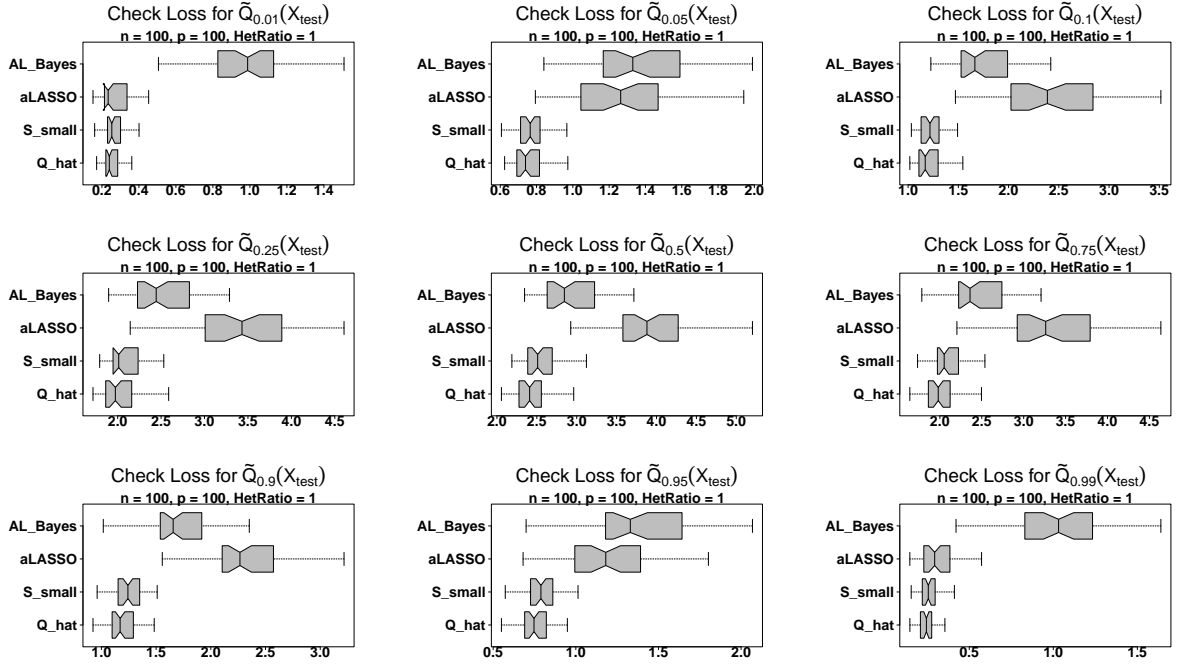


Figure E.11: Check Loss: $n = 200, p = 50, \text{HetRatio} = 0.5$

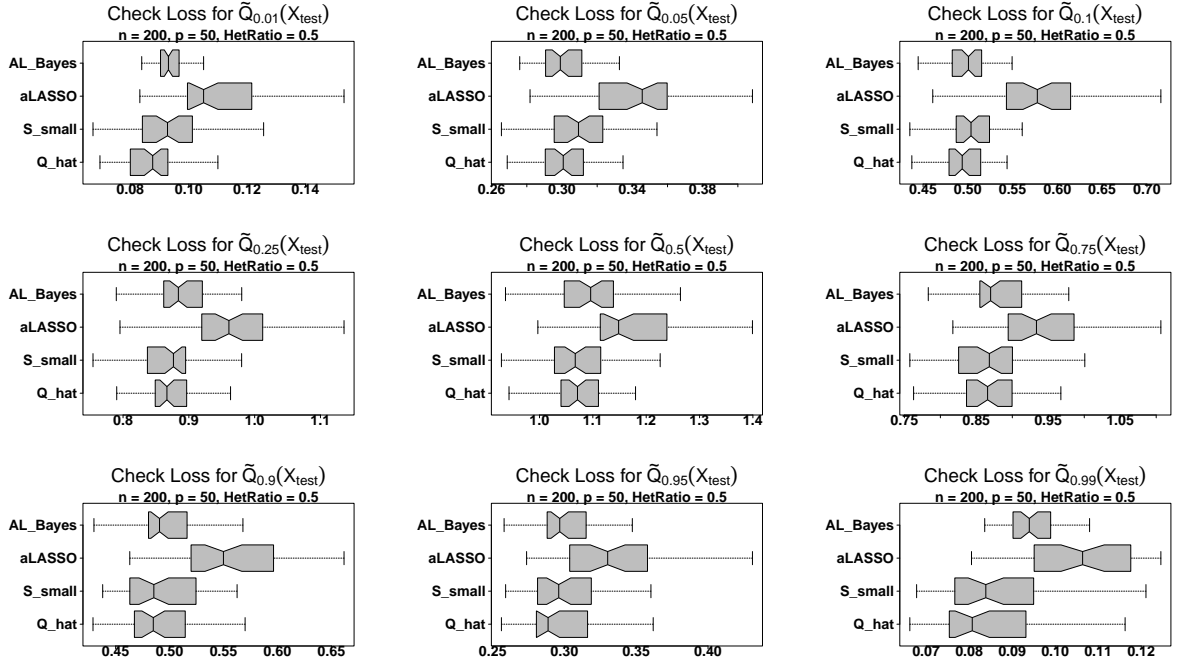
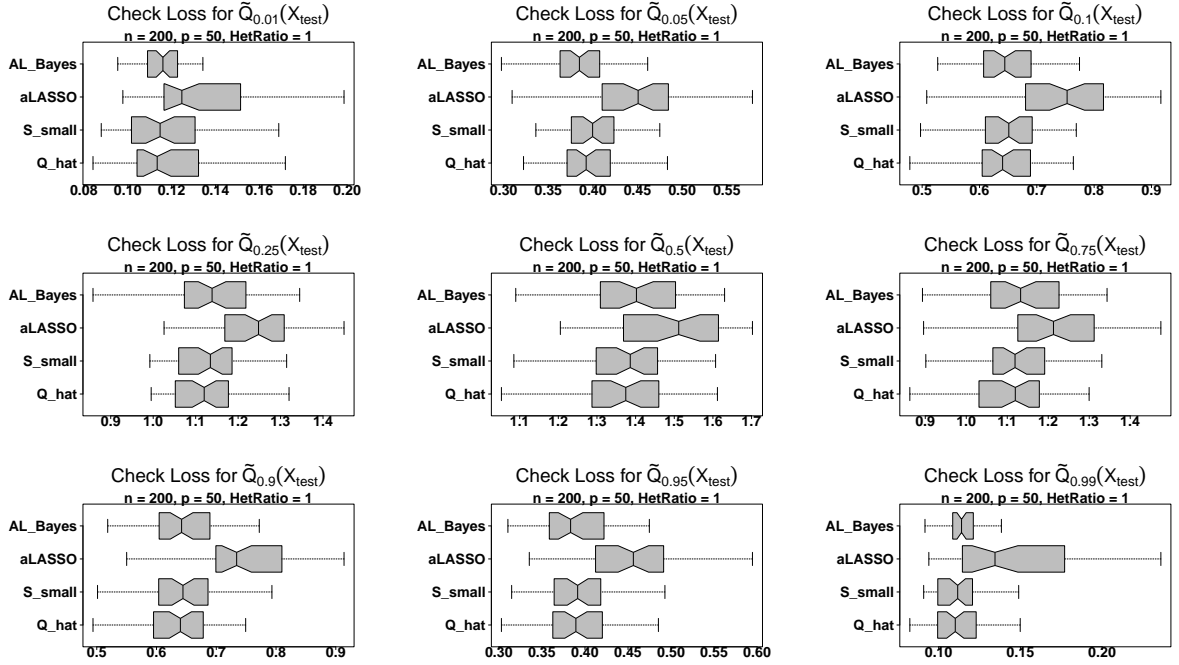


Figure E.12: Check Loss: $n = 200, p = 50, \text{HetRatio} = 1$



Calibration: $n = 500, p = 20, \text{HetRatio} = 0.5$

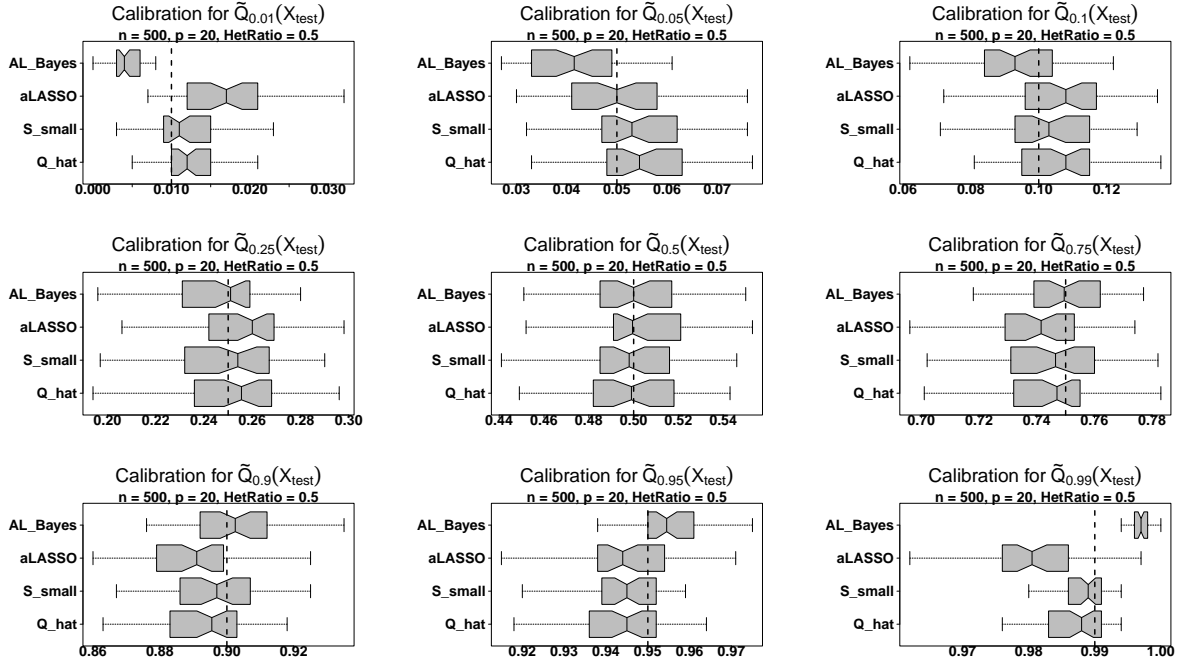
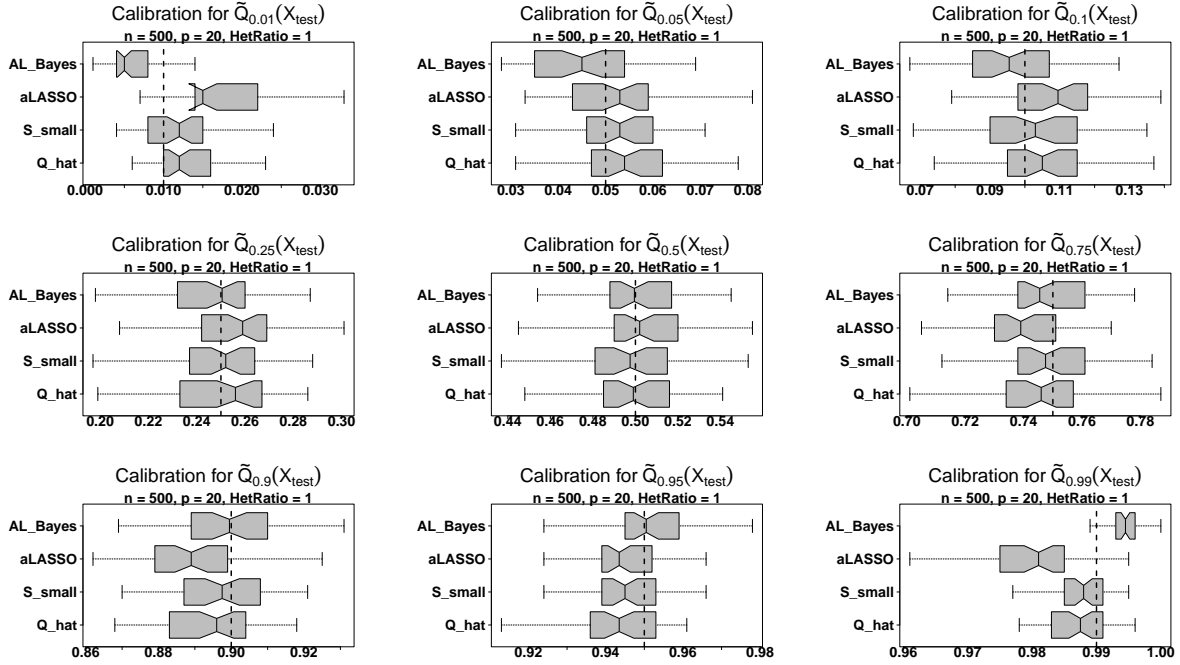


Figure E.13: Calibration: $n = 500, p = 20, \text{HetRatio} = 1$



Calibration: $n = 100, p = 100, \text{HetRatio} = 0.5$

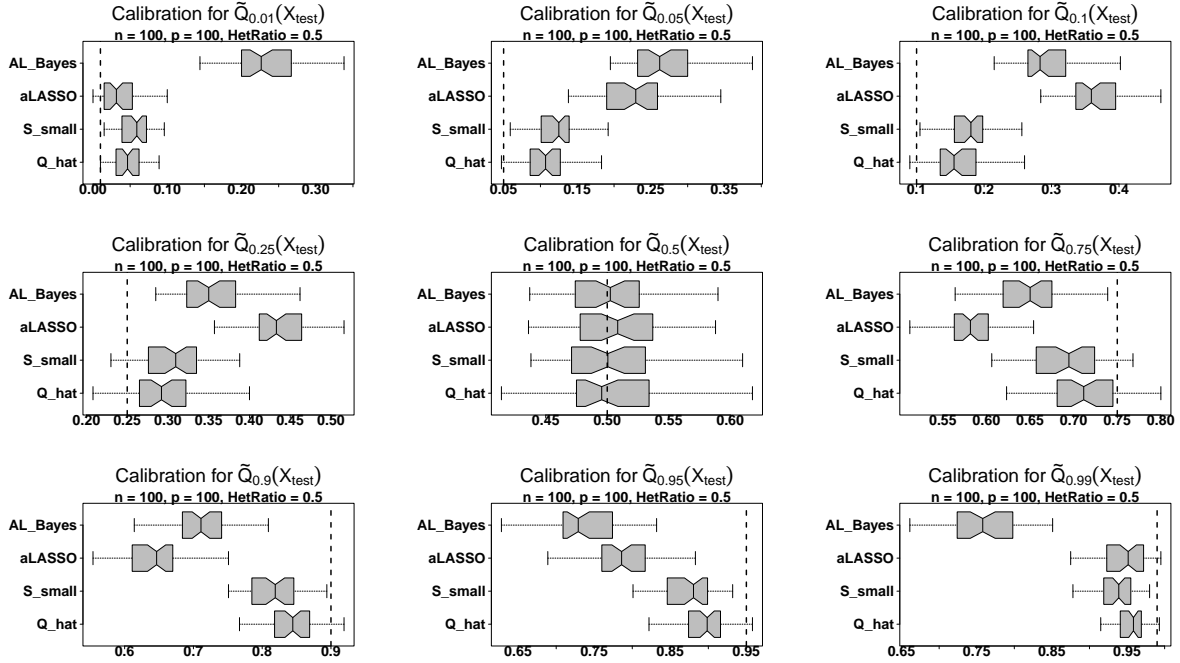


Figure E.14: Calibration: $n = 100, p = 100, \text{HetRatio} = 1$

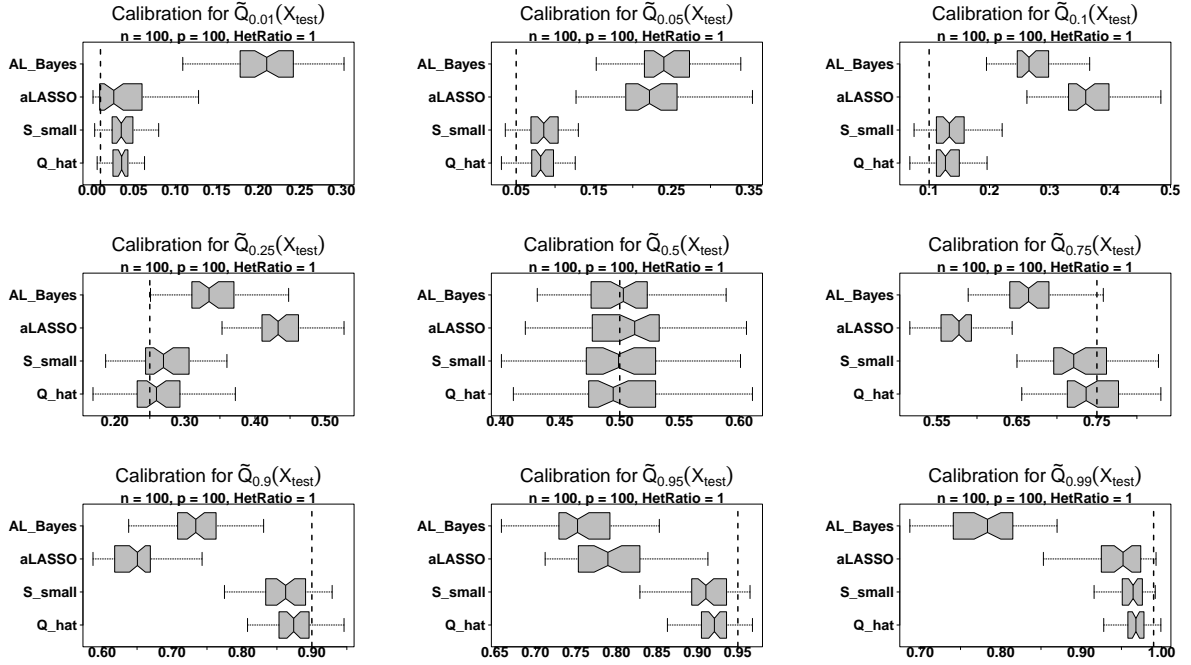


Figure E.15: Calibration: $n = 200, p = 50, \text{HetRatio} = 0.5$

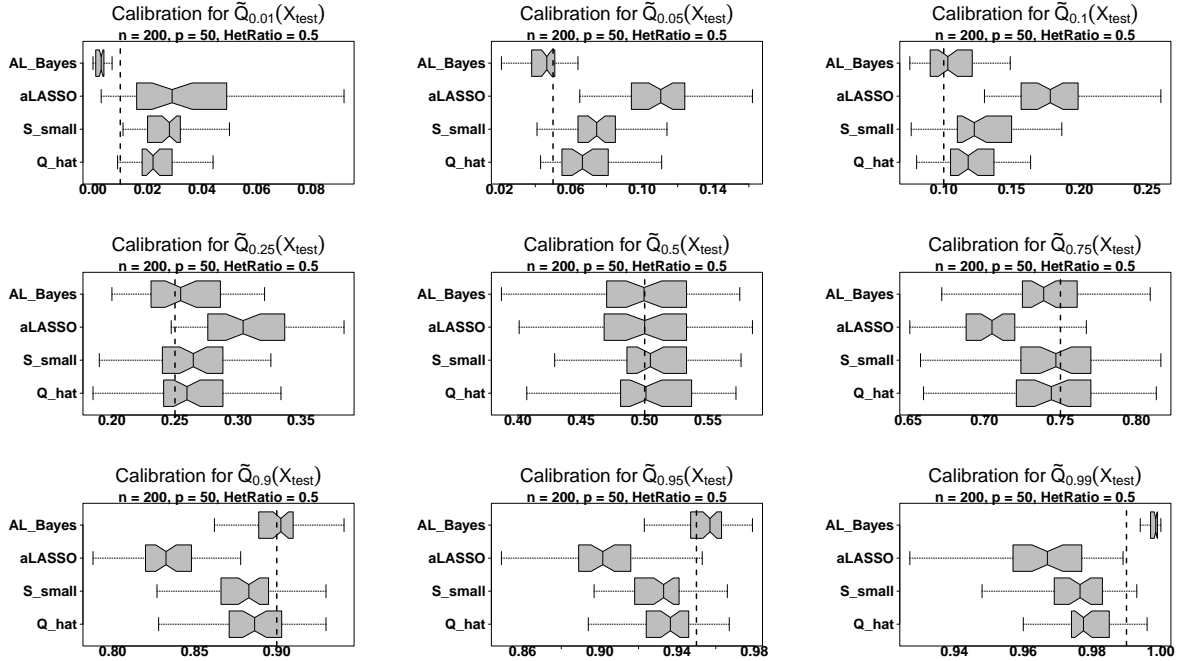
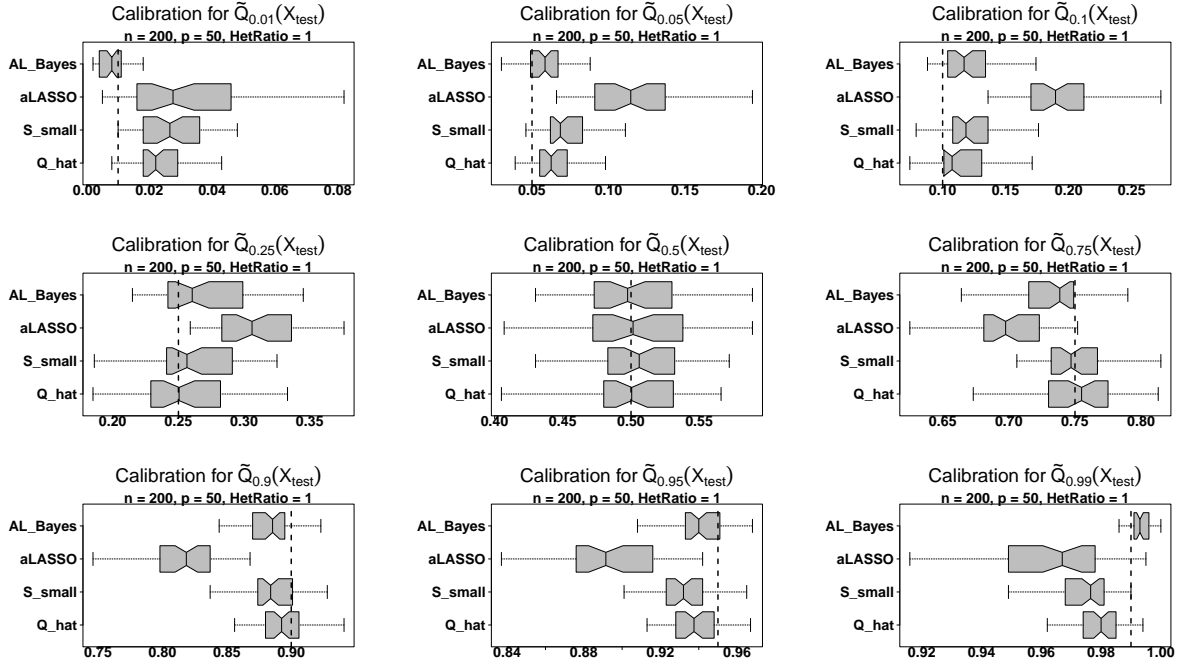


Figure E.16: Calibration: $n = 200, p = 50, \text{HetRatio} = 1$



E.4 Variable Importance

In the main paper, we include results on the variable selection capabilities of the proposed approach based on the single subset $S_{small}(\tau)$ which is a member of each quantile-specific acceptable family $\mathbb{A}_{0.05}(\tau)$. However, a primary advantage of curating acceptable families for any quantile is that it removes reliance on a singular subset for capturing variable importance. As such, we evaluate the variable importance metric $VI_j(\tau)$ (19) across simulation repetitions. This quantity is valuable: it provides an informative summary of the acceptable family (17) that is more comprehensive than any single subset, including $S_{small}(\tau)$.

In each simulation repetition and for each enumerated quantile, we average the variable importance for the homogeneous predictors and the predictors with zero coefficients (*zero*), and compute the variable importance for the single heterogeneous predictor. We average these metrics across simulation repetitions. The results for $n = 200, p = 50, \text{HetRatio} = 1$ are presented in Table 6, with similar results for the other settings, including those with

independent covariates.

By examining $VI_j(\tau)$, we decide that the heterogeneous predictor is nearly vital for prediction of each quantile besides the median, when $\beta_{het}(0.5) = 0$. This is informative, especially in conjunction with Table 2 in the main paper. In the $n = 200, p = 50, \text{HetRatio} = 1$ setting, $S_{small}(\tau)$ does not achieve near 100% true positive rates for any quantile, but variable importance maintains that it is a vital component of the quantile model. In addition, the importance of the homogeneous predictors increases as the magnitude of the heterogeneous predictor decreases. Finally, the zero predictors are deemed non-essential, as seen by low average variable importance. Variable importance computed using the quantile-specific acceptable family expands the analysis beyond a single subset, providing useful and accurate information on informative covariates across the response distribution.

E.5 Quantile Crossing

We also investigate the quantile crossing properties of the competing approaches. Under a coherent probability model for $Y \mid \mathbf{x}$, quantiles cannot cross: $\tilde{Q}_\tau(\mathbf{x}) < \tilde{Q}_{\tau'}(\mathbf{x})$ for any $\tau < \tau'$. However, only the model-based quantiles (Q_{hat}) enforce this property; the competing methods, including the proposed approach, do not explicitly enforce quantile non-crossing. Thus, we seek to quantify the abundance of quantile non-crossing for each method.

For any $\tau < \tau'$, we compute the out-of-sample non-crossing rate (NCR) between neighboring quantile predictions at the testing points:

$$\text{NCR}(\tau, \tau') = n_{test}^{-1} \sum_{i=1}^{n_{test}} \mathbb{1}\{\tilde{Q}_\tau(\mathbf{x}_{test_i}) < \tilde{Q}_{\tau'}(\mathbf{x}_{test_i})\}. \quad (\text{E.1})$$

When $\text{NCR}(\tau, \tau') = 1$, there is no quantile crossing between the τ th and τ' th quantiles.

We compute $\text{NCR}(0.01, 0.05)$ and $\text{NCR}(0.95, 0.99)$ averaged across simulations for each method (Table 7). Remarkably, the proposed approach renders quantile crossing negligible *without* any explicit constraints in the decision analysis for estimation or selection. These

results showcase a key advantage of the Bayesian decision analysis (6): by fitting to the model-based fitted quantiles via (8), the optimal linear actions benefit from the implicit quantile non-crossing of $\hat{Q}_\tau(\mathbf{x})$ under \mathcal{M} . Thus, we (nearly) acquire the primary advantage of simultaneous quantile regression methods (Section 1.2), but without the need for unwieldy constraints. By comparison, the competing frequentist is subject to abundant quantile crossing, especially with larger p and stronger heterogeneity. The Bayesian competitor preserves non-crossing for smaller p settings, but this property is badly violated for $p = 100$. For both methods, this limits the interpretability of the estimated linear coefficients and suggests that the estimated quantiles may be unreliable for prediction or inference.

F North Carolina Data Analysis

F.1 Correlation Among Covariates

Many of the covariates in the augmented North Carolina data set are highly correlated, which is evident in Figure F.1. This promotes the collection of many, near-optimal and competing explanations for the same quantile function.

F.2 Evaluating the LL-LS Model Fit on the North Carolina Data

Prior to posterior summarization, it is vital to first ensure that the Bayesian model \mathcal{M} , which is specified as the LL-LS model (21), is calibrated to the North Carolina data. To do so, we utilize posterior predictive QQ-plots (Pratola et al., 2020). Under a well-calibrated model, the quantiles of the observed response variables at each covariate value under the posterior predictive distribution should be approximately uniform. For each covariate value we generate 2500 draws from the corresponding posterior predictive distribution of reading scores using posterior samples from the LL-LS model. We then calculate the empirical quantiles of the observed response at each covariate value based on the posterior predictive draws. The ordered sample quantiles of the observed reading scores are plotted against

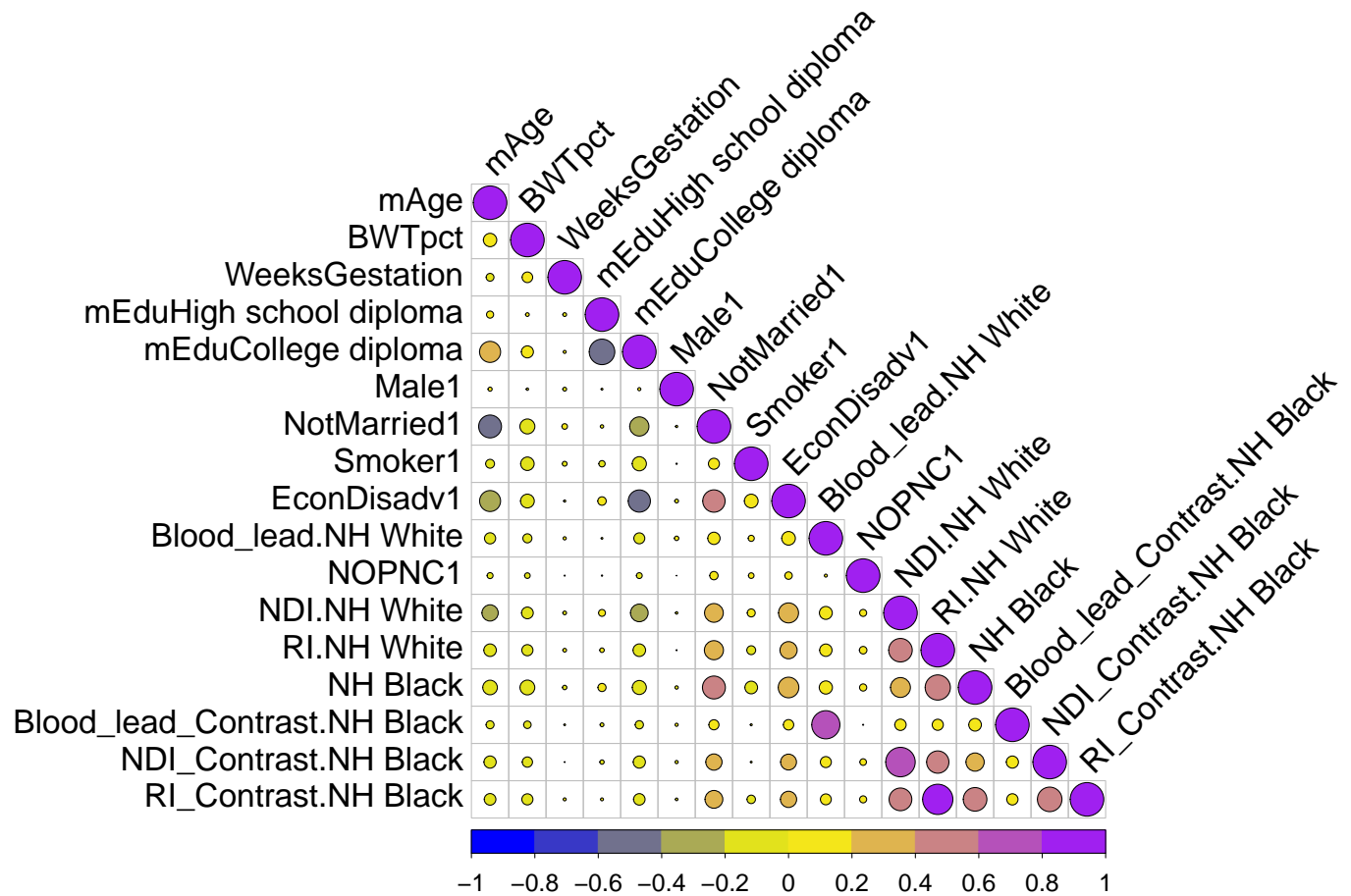


Figure F.1: Pairwise pearson's correlation between covariates in the North Carolina data. Varying degrees of association can be observed. Thus, interchanging highly correlated predictors in linear quantile regression will likely sacrifice little predictive power. This supports the curation of acceptable families for each quantile.

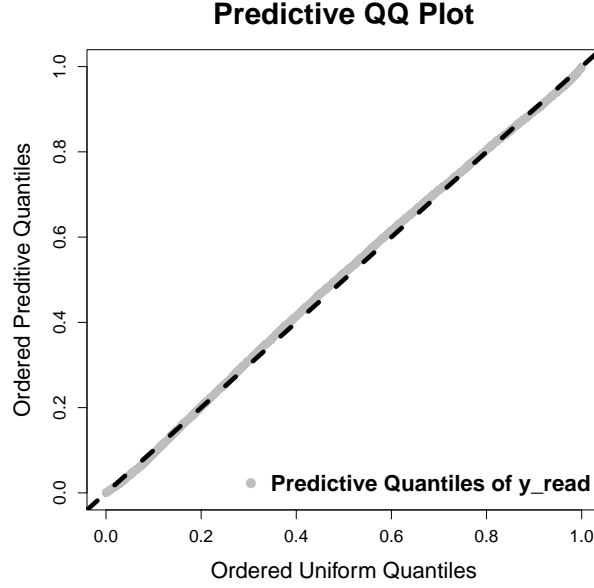


Figure F.2: Predictive QQ plot for reading scores under the LL-LS model. Because the predictive quantiles of the observed reading scores are approximately uniform, as evidenced by little deviation from the 45-degree line, the model is approximately calibrated to the data.

uniform quantiles in Figure F.2. Overlaid onto the plot is 45-degree line. We observe that the sample quantiles are approximately uniform, providing evidence that the LL-LS model is calibrated to the data.

We next determine the extent to which the North Carolina data displays predictor-dependent heteroscedasticity, which motivates a quantile regression analysis. We base our comparisons to a Bayesian homoscedastic linear regression (BHLR) fit to the North Carolina data using the same predictors and response, which assumes constant variance for any covariate value. We specify independent horseshoe priors on the BHLR regression coefficients (?), and an inverse gamma prior on the error variance.

For these comparisons, traditional metrics like root mean squared error (RMSE) are unsatisfying since they are geared toward estimating predictive power, rather than the quality of a model’s higher order properties. Thus, we rely on graphical displays of the variance process to determine whether the LL-LS model better detects predictor-dependent heteroscedasticity over BHLR. If the variance in end-of-grade reading scores can be explained by the covari-

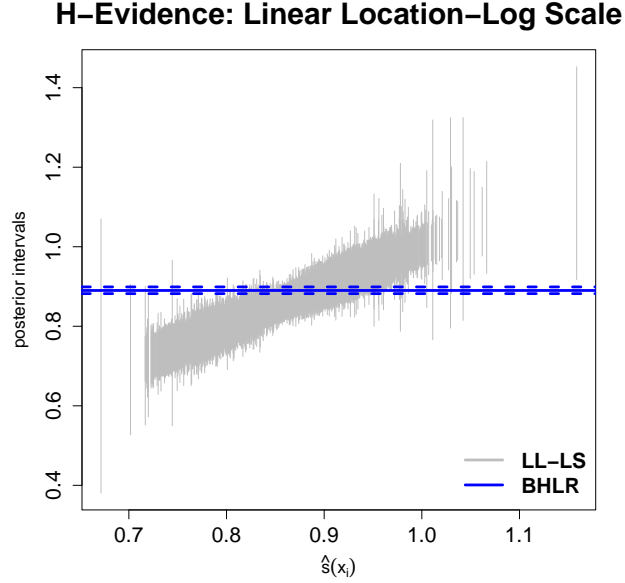


Figure F.3: H-evidence for the linear location-log scale model \mathcal{M} . Relative to homoscedastic linear regression, \mathcal{M} provides evidence that the error variance is predictor dependent, as evidenced by the significant number of posterior intervals for $\{s(\mathbf{x}_i)\}$ that do not overlap with the homoscedastic estimate.

ates in our data set, we hypothesize that the model-based conditional quantiles will have heterogeneous covariates effects.

We summarize the variance process under the LL-LS model using an *H-evidence* plot (Pratola et al., 2020) in Figure F.3, which plots 95% posterior intervals for $\{s(\mathbf{x}_i)\} = \{\sigma \exp(\mathbf{x}_i^\top \boldsymbol{\gamma})\}$. We further sort these intervals by their posterior means $\hat{s}(\mathbf{x}_i)$ which aids in visualization. By comparing the estimates of $\{s(\mathbf{x})\}$ under the LL-LS to the constant error variance estimate obtained from BHLR, we detect whether there is sufficient evidence in the data to determine that $s(\mathbf{x})$ is non-constant. Thus, we overlay onto the intervals the posterior mean of the error variance under the BHLR, with accompanying 95% credible bands.

Figure F.3 provides evidence that the variance is heteroscedastic: many of the posterior intervals for $\{s(\mathbf{x}_i)\}$ do not overlap with the constant variance estimator under BHLR. As such, we anticipate that linear summaries of the model-based conditional quantiles will uncover covariates for which estimated quantile regression coefficients $\boldsymbol{\beta}_j(\tau)$ vary in τ .

F.3 Posterior Summarization of the Bayesian Quantile Regression

We also conducted the proposed quantile regression with subset selection using posterior samples from Bayesian quantile regression under the asymmetric Laplace likelihood with adaptive LASSO priors on the regression coefficients. We evaluate the sensitivity of the variable importance and quantile-specific smallest acceptable subsets to the underlying Bayesian model.

Given the wide posterior uncertainty under this model for the quantile regression coefficients under the Bayesian quantile regression, particularly for extreme quantiles (Figures 2 - 3), we curate quantile-specific acceptable families using $\varepsilon = .25$ for $\tau = \{0.01, 0.99\}$ and $\varepsilon = .10$ for the other quantiles. This enforces that there be stronger evidence under the model that each subset fits better than the anchor. In addition, we extract 80% credible intervals under the posterior action to quantify uncertainty among the covariates included in $S_{small}(\tau)$.

We first present the marginal variable importance for each covariate from the quantile-specific acceptable families, and compare these to Figure 4 in the main paper in Figure F.4. We observe between the models that the metrics are similar for each covariate.

Furthermore, the variables included in at least one $S_{small}(\tau)$ across the variables were identical between the LL-LS model and the Bayesian quantile regression. We compare the inference under the posterior action between the two models for the main effect covariates in Figure F.6. The effect sizes and directionality across τ are quite similar. Notably, the non-monotone pattern across quantiles observed under the posterior inference for **AL_Bayes** in Figure 2 is now partially corrected for **EconDisadv** and **mRace**.

To complete the analysis, we include comparisons of the inference for the interaction terms between smallest acceptable subsets, as was done in Figure 3 in the main paper.

For these coefficients, S_{small} obtained via the Bayesian quantile regression detects heterogeneity across quantiles for **Blood_lead** and **NDI**, and provides evidence of interactions

between both NDI and RI with **mRace**. This is consistent with S_{small} obtained under the LL-LS model. However, S_{small} under the Bayesian quantile regression does not include as many of these interactive effects across quantiles, which is due to the wide posterior uncertainty under the Bayesian quantile regression model which causes acceptable summaries to be generally more sparse.

Algorithm 1 Bayesian quantile regression, inference and subset selection using posterior summarization

1. Fit a Bayesian regression model \mathcal{M}

- **Description:** Fit a Bayesian model to $\{\mathbf{x}_i, y_i\}_{i=1}^n$ and extract posterior samples of model-based conditional quantile functions at each \mathbf{x}_i and any quantile τ of interest;
- **Inputs:** Observed data $\{y_i, \mathbf{x}_i\}$
- **Outputs:** M posterior samples of model-based conditional quantile functions $\{Q_\tau(Y_i | \mathbf{x}_i, \boldsymbol{\theta}^m)\}_{i=1}^M$
 - In the case of the LL-LS model (21), these samples are easily computed with each posterior sample of $\boldsymbol{\theta}$, e.g. $Q_\tau(Y | \mathbf{x}, \boldsymbol{\theta}^m) = \mathbf{x}^\top \boldsymbol{\xi}^m + \sigma^m \exp(\mathbf{x}^\top \boldsymbol{\gamma}^m) \Phi^{-1}(\tau)$

2a. Quantile estimation and uncertainty quantification

- **Description:** For any τ and subset $S \subseteq \{1, \dots, p\}$ of predictors, apply decision analysis to obtain quantile-specific linear coefficient estimates and uncertainty quantification.
- **Inputs:** Posterior samples $\{Q_\tau(Y_i | \mathbf{x}_i, \boldsymbol{\theta}^m)\}_{m=1}^M$, covariate submatrix \mathbf{X}_S
- **Outputs:** The optimal action (8) with accompanying uncertainty provided by the posterior action (9)
 - For any subset S of predictors, the optimal action is simply given by $(\mathbf{X}_S^\top \mathbf{X}_S)^{-1} \mathbf{X}_S^\top \hat{\mathbf{Q}}_\tau(\mathbf{X})$ as in Lemma 2.1. The posterior action is obtained by projecting each draw of $\{Q_\tau(Y_i | \mathbf{x}_i, \boldsymbol{\theta}^m)\}_{i=1}^M$ onto \mathbf{X}_S .

2b. Subset search, filtration, and selection

- **Description:** For any τ , conduct a quantile-specific subset search, accumulate a family of subsets with strong predictive power, and summarize this family via i) a single subset that balances parsimony and predictive power and ii) measures of variable importance across all subsets in the family.
 - **Inputs:** Posterior samples $\{Q_\tau(Y_i | \mathbf{x}_i, \boldsymbol{\theta}^m)\}_{i=1}^M$, covariates \mathbf{X} , m_k for the BBA filtration, and ϵ for the acceptable family criteria.
 - **Outputs:** Posterior samples of (16) for each $S \in \mathbb{S}(\tau)$ obtained from the BBA search, which are used to determine acceptable subsets $\mathbb{A}_{0.05}(\tau)$ based on the criteria outlined by (17). The subset with the smallest cardinality is $S_{small}(\tau)$
 - For the BBA algorithm, the key inputs are simply the point-wise posterior mean of the quantile function $\hat{\mathbf{Q}}_\tau(\mathbf{X})$, the covariates \mathbf{X} and m_k . The output is $\mathbb{S}(\tau)$, which is an $L \times p$ matrix of indicators, with each row corresponding to a subset. The indicators determine the member active predictors in each subset.
 - For each subset in $\mathbb{S}(\tau)$, posterior samples of (16) are obtained by extracting the optimal action for that subset, forming point predictions using that action, and evaluating the posterior distribution of the aggregated squared error loss using samples $\{Q_\tau(Y_i | \mathbf{x}_i, \boldsymbol{\theta}^m)\}_{i=1}^M$. The same process is repeated using the anchor action $\hat{\mathbf{Q}}_\tau(\mathbf{X})$. These samples are combined to measure (16).
 - Acceptable subsets are those whose corresponding posterior distribution of (16) meets the criteria outlined by (17). Variable importance (19) for each variable j is computed by measuring the proportion of subsets which include variable j
-

$n = 200, p = 50, \text{HetRatio} = 0.5$

	τ	0.01	0.05	0.25	0.5	0.75	0.95	0.99
Coverage Rate	$S_{small}(\tau)$	0.92	0.94	0.92	0.91	0.92	0.93	0.91
	S_{full}	0.97	0.97	0.95	0.95	0.95	0.96	0.97
	AL_{Bayes}	0.99	0.98	0.97	0.98	0.97	0.98	0.98
Avg. 95% CI Width	$S_{small}(\tau)$	1.02	0.95	0.81	0.77	0.80	0.94	1.02
	S_{full}	3.56	2.96	2.33	2.18	2.34	2.96	3.57
	AL_{Bayes}	7.87	4.30	2.62	2.33	2.61	4.34	8.30

$n = 500, p = 20, \text{HetRatio} = 1$

	τ	0.01	0.05	0.25	0.5	0.75	0.95	0.99
Coverage Rate	$S_{small}(\tau)$	0.92	0.91	0.90	0.89	0.89	0.94	0.95
	S_{full}	0.93	0.92	0.91	0.91	0.91	0.96	0.97
	AL_{Bayes}	0.94	0.94	0.93	0.94	0.95	0.99	0.99
Avg. 95% CI Width	$S_{small}(\tau)$	0.63	0.51	0.36	0.31	0.37	0.52	0.65
	S_{full}	1.41	1.14	0.83	0.75	0.84	1.15	1.43
	AL_{Bayes}	4.01	2.40	1.43	1.25	1.41	2.42	4.32

$n = 500, p = 20, \text{HetRatio} = 0.5$

	τ	0.01	0.05	0.25	0.5	0.75	0.95	0.99
Coverage Rate	$S_{small}(\tau)$	0.92	0.91	0.89	0.89	0.89	0.91	0.92
	S_{full}	0.93	0.92	0.91	0.90	0.91	0.92	0.94
	AL_{Bayes}	0.95	0.95	0.94	0.94	0.95	0.96	0.98
Avg. 95% CI Width	$S_{small}(\tau)$	0.39	0.34	0.28	0.26	0.29	0.34	0.38
	S_{full}	1.54	1.29	1.05	0.99	1.05	1.30	1.54
	AL_{Bayes}	3.71	2.15	1.29	1.13	1.26	2.19	4.00

$n = 100, p = 100, \text{HetRatio} = 1$

	τ	0.01	0.05	0.25	0.5	0.75	0.95	0.99
Coverage Rate	$S_{small}(\tau)$	0.73	0.73	0.73	0.75	0.73	0.74	0.73
	S_{full}	0.82	0.82	0.82	0.84	0.81	0.82	0.81
	AL_{Bayes}	0.92	0.94	0.96	0.98	0.96	0.93	0.91
Avg. 95% CI Width	$S_{small}(\tau)$	0.44	0.38	0.30	0.25	0.34	0.48	0.51
	S_{full}	2.04	1.69	1.15	1.06	1.18	1.82	2.30
	AL_{Bayes}	6.05	6.9	7.56	7.62	7.50	6.80	5.96

$n = 100, p = 100, \text{HetRatio} = 0.5$

	τ	0.01	0.05	0.25	0.5	0.75	0.95	0.99
Coverage Rate	$S_{small}(\tau)$	0.75	0.76	0.77	0.79	0.77	0.76	0.75
	S_{full}	0.94	0.95	0.95	0.91	0.95	0.96	0.95
	AL_{Bayes}	0.90	0.92	0.94	0.96	0.94	0.91	0.90
Avg. 95% CI Width	$S_{small}(\tau)$	0.57	0.60	0.71	0.71	0.68	0.74	0.66
	S_{full}	2.43	2.05	1.56	1.45	1.58	2.14	2.51
	AL_{Bayes}	3.99	4.74	4.88	4.96	4.86	4.42	3.90

Coverage rates and average widths of 95% credible intervals for the posterior action (9) with $S_{small}(\tau)$ or S_{full} as well as AL_{Bayes} . The intervals for $S_{small}(\tau)$ and S_{full} are significantly more narrow than those for AL_{Bayes} , especially for quantiles near zero or one, and typically maintain nominal coverage. $S_{small}(\tau)$ sacrifices some coverage in favor of sparsity, and thus provides the most narrow intervals.

Table 5: Independent Covariates: $n = 200, p = 50, \text{HetRatio} = 1$

	τ	0.01	0.05	0.25	0.5	0.75	0.95	0.99
TPR	$S_{small}(\tau)$	0.34	0.53	0.75	0.82	0.78	0.62	0.50
	aLASSO	0.14	0.76	0.93	0.95	0.96	0.83	0.25
	AL_{Bayes}	0.00	0.01	0.32	0.49	0.36	0.01	0.00
TNR	$S_{small}(\tau)$	0.84	0.80	0.76	0.75	0.76	0.80	0.84
	aLASSO	0.87	0.48	0.24	0.23	0.34	0.47	0.86
	AL_{Bayes}	1.00	0.99	0.93	0.90	0.93	0.99	1.00

Independent Covariates: $n = 200, p = 50, \text{HetRatio} = 0.5$

	τ	0.01	0.05	0.25	0.5	0.75	0.95	0.99
TPR	$S_{small}(\tau)$	0.87	0.95	0.99	0.98	0.96	0.92	0.89
	aLASSO	0.20	0.91	0.99	1.00	0.99	0.95	0.35
	AL_{Bayes}	0.00	0.00	0.28	0.43	0.31	0.01	0.00
TNR	$S_{small}(\tau)$	0.78	0.75	0.69	0.67	0.69	0.74	0.78
	aLASSO	0.89	0.49	0.26	0.27	0.29	0.49	0.89
	AL_{Bayes}	1.00	0.99	0.91	0.87	0.91	0.99	1.00

Independent Covariates: $n = 500, p = 20, \text{HetRatio} = 1$

	τ	0.01	0.05	0.25	0.5	0.75	0.95	0.99
TPR	$S_{small}(\tau)$	0.98	0.99	0.95	1.00	0.94	0.97	0.97
	aLASSO	0.77	1.00	0.99	1.00	0.99	1.00	1.00
	AL_{Bayes}	0.00	0.58	0.88	1.00	0.88	0.60	0.01
TNR	$S_{small}(\tau)$	0.95	0.94	0.93	0.92	0.93	0.95	0.96
	aLASSO	0.87	0.71	0.57	0.53	0.56	0.72	0.85
	AL_{Bayes}	1.00	1.00	0.99	0.99	0.99	1.00	1.00

Independent Covariates: $n = 500, p = 20, \text{HetRatio} = 0.5$

	τ	0.01	0.05	0.25	0.5	0.75	0.95	0.99
TPR	$S_{small}(\tau)$	0.86	0.86	0.84	1.00	0.84	0.86	0.86
	aLASSO	0.86	0.99	0.95	1.00	0.95	0.98	0.83
	AL_{Bayes}	0.00	0.59	0.80	1.00	0.82	0.66	0.00
TNR	$S_{small}(\tau)$	0.97	0.95	0.93	0.91	0.92	0.95	0.98
	aLASSO	0.87	0.76	0.61	0.56	0.59	0.77	0.86
	AL_{Bayes}	1.00	1.00	0.99	0.99	0.99	1.00	1.00

Independent Covariates: $n = 100, p = 100, \text{HetRatio} = 1$

	τ	0.01	0.05	0.25	0.5	0.75	0.95	0.99
TPR	$S_{small}(\tau)$	0.03	0.04	0.04	0.03	0.04	0.03	0.03
	aLASSO	0.05	0.50	0.84	0.88	0.83	0.47	0.43
	AL_{Bayes}	0.05	0.04	0.05	0.04	0.05	0.05	0.05
TNR	$S_{small}(\tau)$	0.99	0.99	0.98	0.99	0.99	0.99	0.99
	aLASSO	0.97	0.66	0.20	0.17	0.22	0.68	0.98
	AL_{Bayes}	1.00	1.00	0.99	0.99	0.99	1.00	1.00

Independent Covariates: $n = 100, p = 100, \text{HetRatio} = 0.5$

	τ	0.01	0.05	0.25	0.5	0.75	0.95	0.99
TPR	$S_{small}(\tau)$	0.14	0.18	0.22	0.22	0.23	0.16	0.13
	aLASSO	0.05	0.55	0.85	0.88	0.84	0.55	0.04
	AL_{Bayes}	0.09	0.09	0.13	0.13	0.14	0.11	0.10
TNR	$S_{small}(\tau)$	0.97	0.95	0.94	0.95	0.95	0.97	0.97
	aLASSO	0.98	0.70	0.25	0.20	0.26	0.71	0.98
	AL_{Bayes}	0.99	0.99	0.99	0.98	0.98	0.99	0.98

True positive rates (TPR) and true negative rates (TNR) for variable selection averaged across simulations with independent covariates. Once again, the proposed approach ($S_{small}(\tau)$) neatly balances TPR and TNR. Low TPRs for the $n = 100, p = 100$ settings are due to the overwhelmingly strong impact of the covariate with heterogeneous effects, which are five to ten times stronger than those corresponding to homogeneous covariates across quantiles.

Table 6: Average $VI_j(\tau)$: $n = 200, p = 50, \text{HetRatio} = 1$

	τ	0.01	0.05	0.25	0.5	0.75	0.95	0.99
Indices (j)	<i>het</i>	0.97	0.96	0.84	0.44	0.84	0.99	0.99
	<i>hom</i>	0.70	0.77	0.87	0.91	0.87	0.79	0.72
	<i>zero</i>	0.34	0.35	0.36	0.35	0.36	0.35	0.34

Average marginal variable importance for the covariate with heterogeneous effects (*het*), the covariates with homogeneous effects (*hom*) and the variables with no effect (*zero*) on the response distribution (top three rows). The quantile-specific acceptable families demonstrate broad agreement about the importance of the heterogeneous covariate for each quantile. This includes correctly identifying low importance for the median, in which case $\beta_{het}(0.5) = 0$. Furthermore, the importance of the homogeneous covariates increase as the magnitude of $\beta_{het}(\tau)$ decreases. Finally, the zero coefficients are correctly deemed as having marginal importance for each quantile.

Table 7: $n = 200, p = 50, \text{HetRatio} = 1$

	NCR(0.01, 0.05)	NCR(0.95, 0.99)
$S_{small}(\tau)$	0.99	0.99
AL_{Bayes}	0.99	0.99
aLASSO	0.88	0.86

$n = 200, p = 50, \text{HetRatio} = 0.5$

	NCR(0.01, 0.05)	NCR(0.95, 0.99)
$S_{small}(\tau)$	0.99	0.98
AL_{Bayes}	0.99	0.99
aLASSO	0.86	0.85

$n = 500, p = 20, \text{HetRatio} = 1$

	NCR(0.01, 0.05)	NCR(0.95, 0.99)
$S_{small}(\tau)$	0.997	1.00
AL_{Bayes}	0.99	0.99
aLASSO	0.95	0.94

$n = 500, p = 20, \text{HetRatio} = 0.5$

	NCR(0.01, 0.05)	NCR(0.95, 0.99)
$S_{small}(\tau)$	1.00	1.00
AL_{Bayes}	0.99	1.00
aLASSO	0.93	0.94

$n = 100, p = 100, \text{HetRatio} = 1$

	NCR(0.01, 0.05)	NCR(0.95, 0.99)
$S_{small}(\tau)$	0.97	0.97
AL_{Bayes}	0.46	0.64
aLASSO	0.93	0.89

$n = 100, p = 100, \text{HetRatio} = 0.5$

	NCR(0.01, 0.05)	NCR(0.95, 0.99)
$S_{small}(\tau)$	1.00	1.00
AL_{Bayes}	0.35	0.71
aLASSO	0.95	0.94

Quantile non-crossing rates between the 1st and 5th and 95th and 99th quantiles. Unlike aLASSO and the competing Bayesian approach, the proposed approach $S_{small}(\tau)$ renders quantile crossing a non-issue.

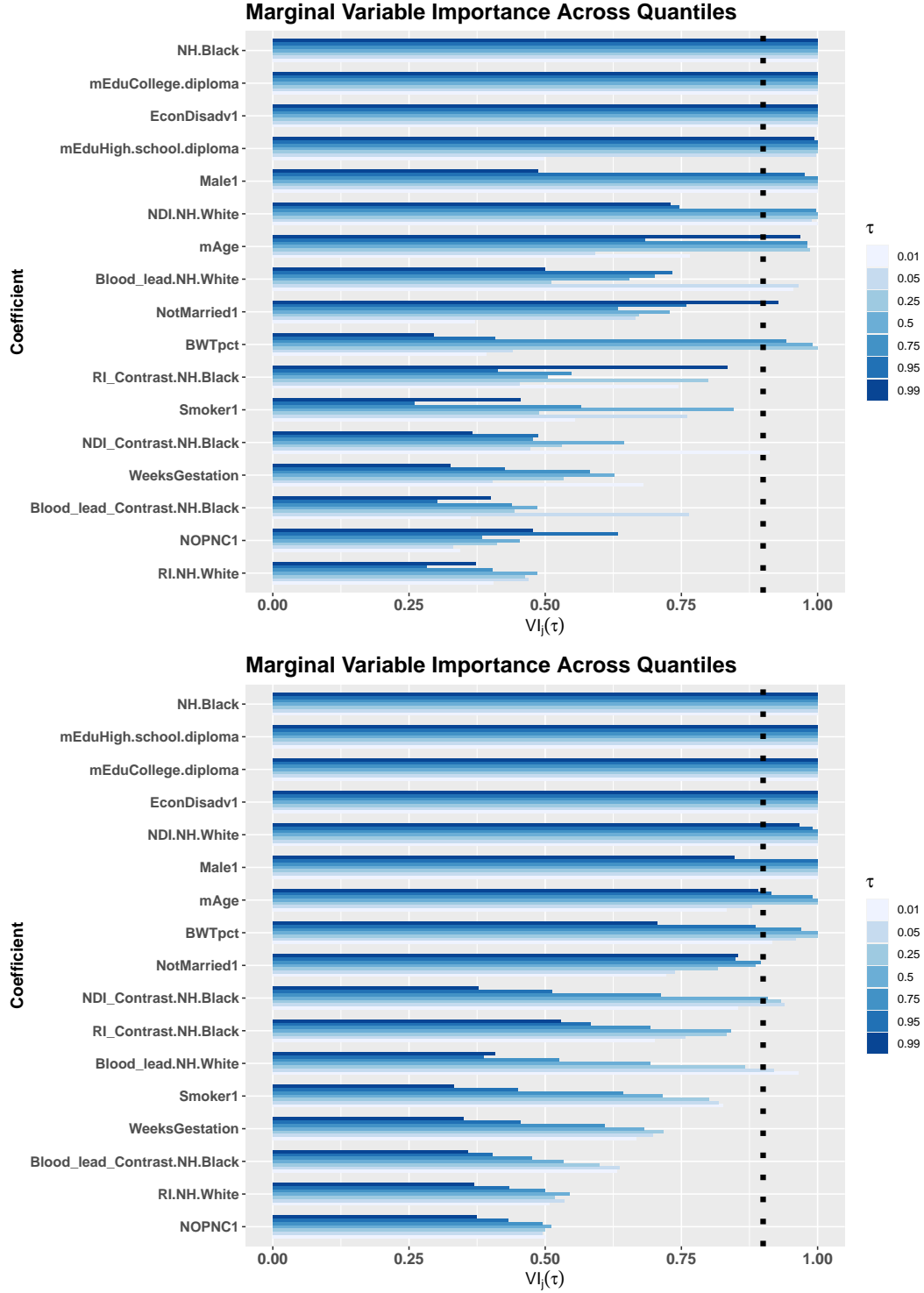


Figure F.4: Variable importance $VI_j(\tau)$ from (19), colored by quantile; the dashed line indicates 0.90. Large values indicate that the covariate appears in many of the acceptable subsets. The top plot provides variable importance under the Bayesian quantile regression, while the bottom row is what is presented in Figure 4 for the LL-LS model. We conclude that overall, the covariates included in the quantile-specific acceptable families are quite similar between the two models.

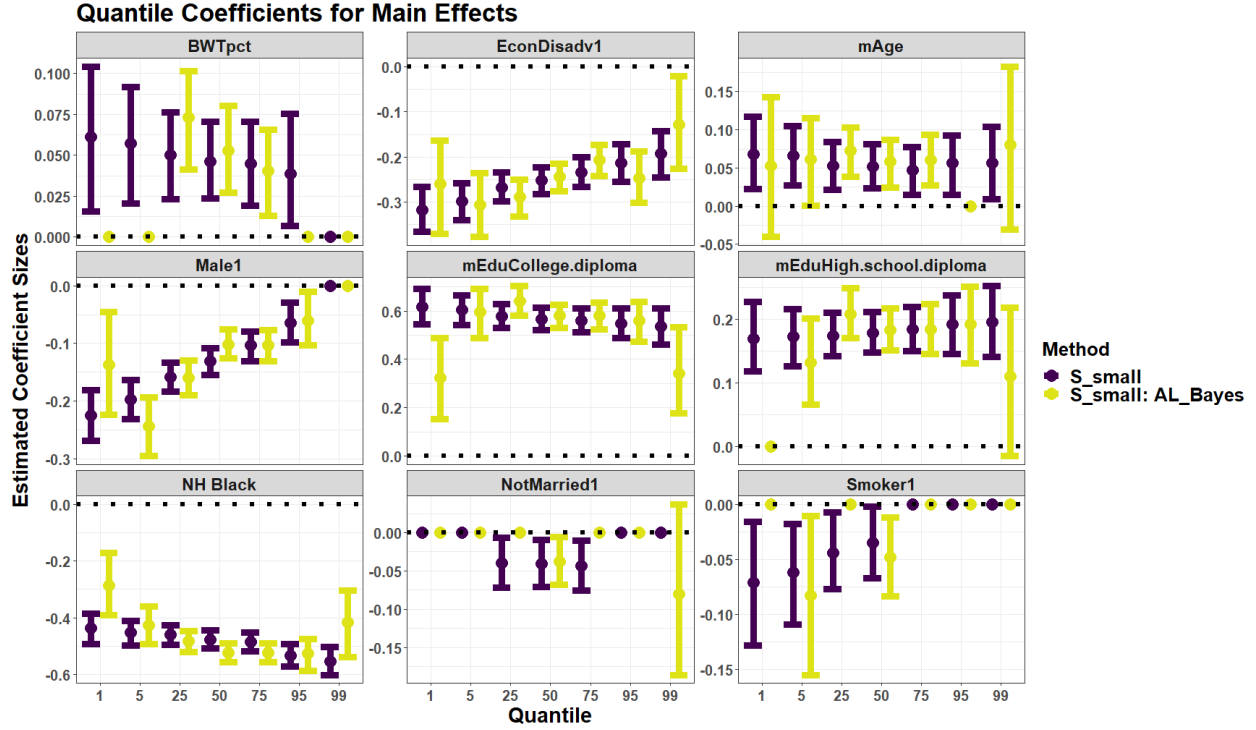


Figure F.5: Inference for the main effects included in at least one quantile-specific smallest acceptable subset obtained through summarization of the LL-LS model and Bayesian quantile regression. The directionality of the coefficients is similar between the two models, while the uncertainty is greater under the Bayesian quantile regression. This is due to the asymmetric laplace likelihood, which does not capture the data generating process as well as the LL-LS model.

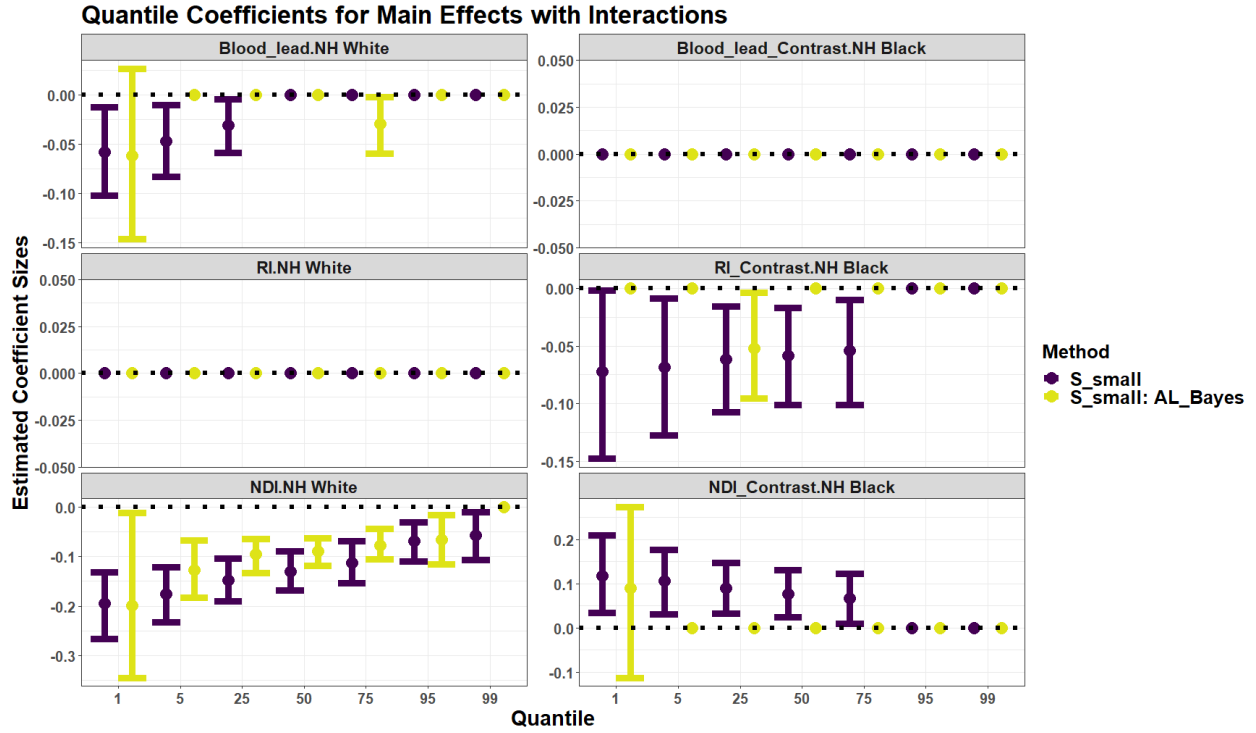


Figure F.6: Inference for quantile regression coefficients obtained through posterior summarization under the LL-LS model and Bayesian quantile regression. The smallest acceptable subset from the Bayesian quantile regression detects heterogeneous effects for Blood_lead and NDI, as well as evidence of interactive effects between both RI and NDI with $mRace$.